Inorganic Chemistry

Article

pubs.acs.org/IC

Dual Emission and Excited-State Mixed-Valence in a Quasi-Symmetric Dinuclear Ru–Ru Complex

Christoph Kreitner,[†,‡] Markus Grabolle,[§] Ute Resch-Genger,[§] and Katja Heinze*[,†]

[†]Institute of Inorganic and Analytical Chemistry, Johannes Gutenberg-University of Mainz, Duesbergweg 10–14, 55128 Mainz, Germany

[‡]Graduate School Materials Science in Mainz, Staudingerweg 9, 55128 Mainz, Germany

[§]Federal Institute for Materials Research and Testing (BAM), Division 1.5, Richard-Willstätter-Str. 11, 12489 Berlin, Germany

Supporting Information

ABSTRACT: The synthesis and characterization of the new dinuclear dipeptide $[(EtOOC\text{-}tpy)Ru(tpy\text{-}NHCO\text{-}tpy)Ru(tpy\text{-}NHCOCH_3)]^{4+}$ $\mathbf{3}^{4+}$ of the bis(terpyridine)ruthenium amino acid $[(HOOC\text{-}tpy)Ru(tpy\text{-}NH_2)]^{2+}$ $\mathbf{1}^{2+}$ are described, and the properties of the dipeptide are compared to those of the mononuclear complex $[(EtOOC\text{-}tpy)Ru(tpy\text{-}NHCOCH_3)]^{2+}$ $\mathbf{4}^{2+}$ carrying the same functional groups. $\mathbf{3}^{4+}$ is designed to serve a high electronic similarity of the two ruthenium sites despite the intrinsic asymmetry arising from the amide bridge. This is confirmed via UV–vis absorption and NMR spectroscopy as well as cyclic voltammetry. $\mathbf{4}^{2+}$ and $\mathbf{3}^{4+}$ are emissive at room temperature, as expected. Moreover, $\mathbf{3}^{4+}$ exhibits dual emission from two different triplet states with different energies and lifetimes at room temperature. This is ascribed to the presence of a unique thermal equilibrium between coexisting $[Ru^{II}(tpy\text{-}NHCO\text{-}tpy^{\bullet-})Ru^{III}]$ and $[Ru^{III}(tpy\text{-}NHCO\text{-}tpy^{\bullet-})Ru^{II}]$ states leading to an unprecedented excited-state $Ru^{II}Ru^{III}$ mixed-valent system via the radical anion bridge $tpy\text{-}NHCO\text{-}tpy^{\bullet-}$. The mixed-valent cation $\mathbf{3}^{5+}$, on the other hand, shows no measurable interaction of the $Ru^{II}Ru^{III}$ centers via the neutral bridge tpy-NHCO-tpy (Robin–Day class I). Reduction of $\mathbf{3}^{4+}$ to the radical cation $\mathbf{3}^{3+}$ by decamethylcobaltocene is bridge-centered as evidenced by rapid-freeze electron paramagnetic resonance spectroscopy. Interestingly, all attempts to observe $\mathbf{3}^{3+}$ via NMR and UV–vis absorption spectroscopy only led to the detection of the diamagnetic complex $\mathbf{3\text{-}H}^{3+}$ in which the bridging amide is deprotonated. Hence $\mathbf{3\text{-}H}^{3+}$ (and $\mathbf{4\text{-}H}^{+}$) appear to reduce protons to dihydrogen. The ease of single and double deprotonation of $\mathbf{4}^{2+}$ and $\mathbf{3}^{4+}$ to $\mathbf{4\text{-}H}^{+}$, $\mathbf{3\text{-}H}^{3+}$, and $\mathbf{3\text{–}2H}^{2+}$ was demonstrated using a strong base and was studied using NMR and UV–vis absorption spectroscopies. The equilibrating excited triplet states of $\mathbf{3}^{4+}$ are reductively quenched by *N*,*N*-dimethylaniline assisted by hydrogen bonding to the bridging amide.

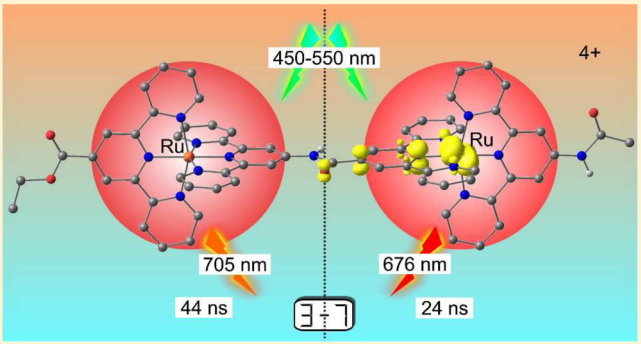

INTRODUCTION

The controlled assembly of multinuclear metal complexes incorporating electrochemically and photochemically active moieties is of great interest for the fundamental understanding of energy and electron transfer[1−3] on a molecular level and the modeling of natural photosynthesis[4] as well as for the design of molecular wires[5,6] and switches,[7,8] photocatalysts,[9−11] and information storage devices.[12] (Polypyridine)ruthenium(II) complexes, especially the archetype compound $[Ru(bpy)_3]^{2+}$ (bpy = 2,2′-bipyridine), have found wide application in such arrays due to their high stability and outstanding photochemical properties. Further applications of this class of compounds comprise photosensitizers in dye-sensitized solar cells[13] and emitters in light-emitting electrochemical cells.[14]

$[Ru(bpy)_3]^{2+}$ features unique optical and electrochemical properties.[15,16] The energetically low-lying π^* orbitals of the heteroaromatic ligands allow for a metal-to-ligand charge transfer (^{1}MLCT) excitation upon irradiation. Rapid intersystem crossing (ISC) leads to population of ^{3}MLCT states.[17] The lowest of these ^{3}MLCT excited states is emissive at room temperature and exhibits a reasonably long lifetime (Φ = 0.095, τ = 855 μs at 298 K in CH_3CN).[16,18] Because of the use of chelating ligands this complex has a fairly high thermal and chemical stability.[19,20]

The use of $[Ru(tpy)_2]^{2+}$ (tpy = 2,2′:6′,2″-terpyridine) instead of $[Ru(bpy)_3]^{2+}$ leads to structurally similar complexes,[21,22] but these compounds have been far less studied and applied in photochemical setups than their bpy analogues. This is due to low emission quantum yields and short excited-state lifetimes at room temperature in fluid solution because the ^{3}MLCT states can undergo thermal depopulation via ^{3}MC states followed by vibrational relaxation and ISC to the ground state.[1,23−25] This hampers the use of these complexes in the fields of photoelectron or energy transfer. Several attempts have been carried out to increase emission lifetimes and quantum

Received: August 21, 2014
Published: November 20, 2014

yields of bis(tridentate)ruthenium(II) complexes. Increasing the bite angle (N−Ru−N) within the ligands raises the energy of the ^{3}MC states through better overlap of ligand and metal orbitals thus shifting the thermal population in favor of the ^{3}MLCT states.[26−30] Functionalization of the parent $[Ru(tpy)_2]^{2+}$ in the 4′ position with push−pull substituents has a similar effect: electron-withdrawing substituents lower the energy of the ^{3}MLCT states, while electron-donating groups increase the energy of the ^{3}MC states.[24,25,31] Emission can be intensified by several orders of magnitude via these approaches.

A major advantage of $[Ru(tpy)_2]^{2+}$ over $[Ru(bpy)_3]^{2+}$ for functionalization in the ligand backbone is the lack of a stereocenter in the former. This is important for the development of multinuclear assemblies as it simplifies synthesis and purification significantly. It becomes evident considering the stereogenic character of $[Ru(bpy)_3]^{2+}$. Its D_3 symmetry leads to enantiomers in the parent complex (Δ, Λ). Complexes of the type $[Ru(bpy)(bpy\text{-}R)(bpy\text{-}R')]^{2+}$, with bpy-R and bpy-R′ carrying different functional groups, result in a mixture of diastereomers that requires sophisticated methods to be separated or avoided.[32−35] Employing $[Ru(bpy)_3]^{2+}$ in dinuclear systems gives rise to three stereoisomers (ΔΔ, meso-ΔΛ, and ΛΛ) that can only be circumvented under certain conditions.[33]

This is why we employed donor- and acceptor-functionalized tpy ligands to develop emissive complexes of the type $[Ru(tpy\text{-}R)(tpy\text{-}R')]^{2+}$.[31,36,37] Using the functional groups R = COOH and R′ = NH_2 gives rise to the metallo amino acid $\mathbf{1}^{2+}$[31] in which the metal is placed in one line with the functional groups thus maximizing the ligands' electronic effects. Amino acid building blocks of this type allow the synthesis of oligopeptides in which ruthenium takes a unique position by enhancing the electronic communication between the building blocks,[31,38−40] which is not observed when the metal is placed in a side chain of the peptide structure.[41−43]

In the work presented herein, we demonstrate the synthesis and characterization of a protected dinuclear dipeptide $[(R\text{-}tpy)Ru(tpy\text{-}NHCO\text{-}tpy)Ru(tpy\text{-}R')]^{4+}$ of the ruthenium amino acid $\mathbf{1}^{2+}$. Dinuclear mixed-valent ruthenium complexes have been widely studied in terms of electronic interaction between the metal centers. Symmetric complexes, especially the Creutz−Taube ion $[(NH_3)_5Ru\text{-}(\mu\text{-}pz)\text{-}Ru(NH_3)_5]^{5+}$ (pz = pyrazine) as prototype,[44] with identical electronic environments around both metal sites have been extensively examined,[45−47] and the theoretical background is well-understood.[48−50] The strength of the through-bond electronic interaction is dominated by the distance between the redox centers, as well as the planarity and appropriate symmetry of the bridging ligand.[51] Additionally, the frontier orbitals of the bridge need to be in a similar energy range as the involved metal orbitals for the interaction to be significant.[45,47,51] A classification into three classes (Robin−Day) distinguishes the degree of communication between the redox centers, with class I being ascribed to noninteracting and class III ascribed to strongly coupled systems.[52−54]

Directional electronic coupling through asymmetric bridging ligands has not been studied in great detail mainly because of the difficulty to generate distinct asymmetric structures[55] that meet the basic requirements for electronic interaction (planarity, sufficiently short distances). Electron transfer in natural systems, on the other hand, always occurs directionally with small driving forces.[56] This is why systematic synthesis and investigation of structurally asymmetric but nearly redox-symmetric mixed-valent systems is of general interest.

We had previously reported the unprotected dipeptide $[(R\text{-}tpy)Ru(tpy\text{-}NHCO\text{-}tpy)Ru(tpy\text{-}R')]^{4+}$, R = COOH, R′ = NH_2 $\mathbf{2}^{4+}$.[57] Its mixed-valent state $\mathbf{2}^{5+}$ features two electronically uncoupled ruthenium moieties due to differing local redox potentials leading to an intrinsic electronic asymmetry. No evidence of photochemical electron transfer from the Ru^{II} moiety onto the Ru^{III} species was found (Robin−Day class I). In contrast to $\mathbf{1}^{2+}$, $\mathbf{2}^{4+}$ containing both a carboxylic acid and an amino group has not been explored in terms of acid−base chemistry, although interesting properties can arise from the combination of redox and acid−base active centers in a single molecule (e.g., proton-coupled electron transfer).[58−60]

In this work, we present an intrinsically structurally asymmetric but, in terms of local redox potentials, highly symmetric derivative of $\mathbf{2}^{4+}$, with R = COOEt and R′ = $NHCOCH_3$ ($\mathbf{3}^{4+}$). Its unique electronic and optical properties are studied in detail and are compared to a closely related mononuclear derivative of the ruthenium amino acid of the form $[(R\text{-}tpy)Ru(tpy\text{-}R')]^{2+}$ (R = COOEt, R′ = $NHCOCH_3$, $\mathbf{4}^{2+}$) with the same terminal functional groups as $\mathbf{3}^{4+}$. The extent of electronic coupling between the redox moieties is evaluated in the neutral, singly oxidized, and singly reduced states as well as in the excited state.

Typically, aliphatic and aromatic amides exhibit only weakly acidic behavior ($pK_a \approx 18-22$ in dimethyl sulfoxide).[61] However, inserting amide bonds in between charged polypyridine ruthenium(II) complexes leads to a substantial polarization of the amide and an acidification of the N−H bond, which is why the acid−base chemistry of $\mathbf{3}^{4+}$ is investigated as well.

EXPERIMENTAL SECTION

General Procedures. Chemicals were obtained from commercial suppliers and were used without further purification. Bis(terpyridine)-ruthenium(II) complexes $[(HOOC\text{-}tpy)Ru(tpy\text{-}NH_2)](PF_6)_2$ $\mathbf{1}(PF_6)_2$, $[(EtOOC\text{-}tpy)Ru(tpy\text{-}NHCOCH_3)](PF_6)_2$ $\mathbf{4}(PF_6)_2$, and $[(EtOOC\text{-}tpy)Ru(tpy\text{-}NH_2)](PF_6)_2$ $\mathbf{5}(PF_6)_2$ were synthesized according to literature-known procedures.[31,36,37] Air- or moisture-sensitive reactions and compounds were handled in dried glassware under an inert gas atmosphere (argon, quality 4.6). Acetonitrile was refluxed over CaH_2 and distilled under argon prior to use in these reactions. IR spectra were recorded on a BioRad Excalibur FTS 3000 spectrometer using cesium iodide disks. UV−vis absorption spectra were recorded on a Varian Cary 5000 spectrometer in 1 cm cuvettes. Emission spectra were recorded on a Varian Cary Eclipse spectrometer. Quantum yields were determined by comparing the areas under the emission spectra recorded for solutions of the samples and a reference with matching absorbances on an energy scale ($\phi([Ru(bpy)_3]Cl_2) = 0.094$ in deaerated CH_3CN).[18] Experimental uncertainty is estimated to be 15%. Luminescence decay curves of the samples in acetonitrile were measured under ambient conditions or under inert atmosphere by time-correlated single-photon counting (TCSPC) at 22 °C under magic-angle conditions with an Edinburgh Instruments lifetime spectrometer (FLS 920) equipped with a supercontinuum laser (SC400-PP, Fianium) in combination with a double monochromator, a MCP-PMT (R3809U-50, Hamamatsu), and a TCSPC module (TCC 900). The instrument response time was 200 ps; the repetition rate was 5 MHz. Sample excitation was at 504 and 492 nm, and fluorescence decays were measured at 684 and 690 nm for $\mathbf{3}(PF_6)_4$ and $\mathbf{4}(PF_6)_2$, respectively. Decay times were obtained from single- or biexponential fits using the spectrometer software. Electrospray ionization (ESI^+) and high-resolution (HR) ESI^+ mass spectra were recorded on a Micromass QTof Ultima API mass spectrometer with analyte solutions in acetonitrile. ESI^+ mass spectra are reported giving the m/z ratio and relative intensity of the most intense peak of the typical ruthenium isotope pattern, while HR ESI^+ numbers are given

dx.doi.org/10.1021/ic5020362 | Inorg. Chem. 2014, 53, 12947−12961

for the lowest m/z ratio in a given ruthenium isotope pattern. Elemental analyses were performed by the microanalytical laboratory of the chemical institutes of the University of Mainz. NMR spectra were obtained with a Bruker Avance II 400 spectrometer at 400.31 (^{1}H), 100.66 (^{13}C), and 376.60 MHz (^{19}F) at 25 °C. Chemical shifts δ [ppm] are reported with respect to residual solvent signals as internal standards (^{1}H, ^{13}C) or external standards (^{19}F): CD_3CN $\delta(^1H)$ = 1.94 ppm, $\delta(^{13}C)$ = 1.32 and 118.26 ppm,[62] $CFCl_3$ $\delta(^{19}F)$ = 0.00 ppm. Electrochemical experiments were performed with a BioLogic SP-50 voltammetric analyzer using platinum wire working and counter electrodes and a 0.01 M $Ag/AgNO_3$ reference electrode. Measurements were carried out at a scan rate of 100 mV s^{-1} for cyclic voltammetry experiments and at 10 mV s^{-1} for square-wave voltammetry experiments using 0.1 M [nBu$_4$N][PF$_6$] as supporting electrolyte in acetonitrile. Potentials are given relative to the ferrocene/ferrocenium couple (0.40 V vs SCE,[63] $E_{1/2}$ = 0.90 ± 5 mV under the given conditions). Electron paramagnetic resonance (EPR) spectra were recorded on a Miniscope MS 300 X-band CW spectrometer (Magnettech GmbH, Germany). Values of g are referenced to Mn^{2+} in ZnS as external standard (g = 2.118, 2.066, 2.027, 1.986, 1.946). Simulations were performed with the EasySpin program package.[64]

Density functional theoretical (DFT) calculations were carried out using the Gaussian09/DFT series of programs[65] employing B3LYP as functional.[66] The choice of functional was made due to the vast abundance of publications using this functional in calculations on transition metal compounds. Previously published theoretical results on mono- and oligonuclear donor−acceptor functionalized [Ru(tpy)$_2$] complexes were in good agreement with the experimental data.[29,39,40,57] The LANL2DZ implementation of Gaussian09 was used as basis set for all atoms. It comprises Dunning/Huzinaga's D95 V valence double-ξ basis without polarization functions for hydrogen, carbon, nitrogen, and oxygen[67] and a Los Alamos effective core potential approach plus valence double-ξ basis for ruthenium.[68−70] This rather small basis set combination was chosen to manage the computational effort of the large systems under study. To account for solvent effects a polarized continuum model modeling acetonitrile solution was used (IEFPCM, acetonitrile).[71−73] Explicit counterions and/or solvent molecules were not taken into account. All structures were characterized as local minima of the potential energy surface by vibrational analysis (N_{imag} = 0). No symmetry constraints were imposed on the molecular geometries.

Synthetic Procedures. *Synthesis of* ***6***$(PF_6)_2$.[57] [(HOOC-tpy)Ru(tpy-NH$_2$)](PF$_6$)$_2$ **1**(PF$_6$)$_2$[31] (339 mg, 0.370 mmol) was suspended in acetyl chloride (25 mL) and refluxed for 2 h giving a dark red solution. Acetyl chloride was distilled from this, and the residual solid was dissolved in acetonitrile. The crude product was triturated by addition of excess diethyl ether and collected via filtration. It was dissolved again in boiling water (250 mL) to cleave the mixed anhydride formed in the reaction of the carboxyl group with acetic anhydride and precipitated after addition of a solution of NH_4PF_6 (250 mg) in water (1 mL). The precipitate was collected, washed with water, and dried under reduced pressure to give [(HOOC-tpy)Ru(tpy-NHCOCH$_3$)](PF$_6$)$_2$ **6**(PF$_6$)$_2$ as a red powder. Yield: 330 mg (0.350 mmol, 95%). Anal. Calcd for $C_{33}H_{25}F_{12}N_7O_3P_2Ru$ (958.6)·4H$_2$O: C, 38.46; H, 3.23; N, 9.51. Found: C, 38.63; H, 3.13; N, 9.68%. Mass spectrometry (MS) (ESI$^+$): m/z (%) = 334.6 (30) [M-2PF$_6$]$^{2+}$, 814.1 (100) [M-PF$_6$]$^+$, 1293.1 (3) [3M-2PF$_6$]$^{2+}$, 1772.6 (3) [4M-2PF$_6$]$^{2+}$. HR-MS (ESI$^+$, m/z): calcd. for $C_{33}H_{25}F_6N_7O_3PRu$ [M-PF$_6$]$^+$: 808.0737; found: 808.0732. ^{1}H NMR (CD_3CN): δ = 9.42 (s, 1H, NH), 9.17 (s, 2H, H^2), 8.94 (s, 2H, H$^{2'}$), 8.62 (d, $^3J_{HH}$ = 8 Hz, 2H, H^5), 8.37 (d, $^3J_{HH}$ = 8 Hz, 2H, H$^{5'}$), 7.97−7.82 (m, 4H, H^6, H$^{6'}$), 7.46−7.41 (m, 2H, H^8), 7.28−7.15 (m, 4H, H^7, H$^{8'}$), 7.12−7.06 (m, 2H, H$^{7'}$), 2.35 (s, 3H, CH_3).

Synthesis of ***7***$(PF_6)_2$. [(HOOC-tpy)Ru(tpy-NHCOCH$_3$)](PF$_6$)$_2$ **6**(PF$_6$)$_2$ (200 mg, 0.209 mmol) was dissolved in absolute acetonitrile (15 mL), and pentafluorophenol (46.2 mg, 0.251 mmol) and *N*,*N*′-diisopropylcarbodiimide (31.7 mg, 0.251 mmol) were added. After it stirred at room temperature for 90 min, the reaction mixture was concentrated to 5 mL under reduced pressure, and the product was triturated by addition of a solution of NH_4PF_6 (297 mg) in water (70 mL). The product was collected via filtration, washed with small amounts of water and diethyl ether, and dried under reduced pressure to give [(C_6F_5OOC-tpy)Ru(tpy-NHCOCH$_3$)](PF$_6$)$_2$ **7**(PF$_6$)$_2$ as red powder. Yield: 217.5 mg (0.193 mmol, 93%). Anal. Calcd for $C_{39}H_{24}F_{17}N_7O_3P_2Ru$ (1124.6)·2H$_2$O: C, 40.36; H, 2.43; N, 8.45. Found: C, 40.24; H, 2.21; N, 8.61%. MS (ESI$^+$): m/z (%) = 417.6 (15) [M-2PF$_6$]$^{2+}$, 834.1 (3) [M-2PF$_6$−H]$^+$, 980.1 (100) [M-PF$_6$]$^+$, 1542.6 (3) [3M-2PF$_6$]$^{2+}$, 2103.6 (3) [4M-2PF$_6$]$^{2+}$. HR-MS (ESI$^+$, m/z): calcd. for $C_{39}H_{24}F_{11}N_7O_3PRu$ [M-PF$_6$]$^+$: 974.0579; found: 974.0562. ^{1}H NMR (CD_3CN): δ = 9.54 (s, 1H, NH), 9.38 (s, 2H, H^2), 9.01 (s, 2H, H$^{2'}$), 8.70 (d, $^3J_{HH}$ = 8 Hz, 2H, H^5), 8.42 (d, $^3J_{HH}$ = 8 Hz, 2H, H$^{5'}$), 7.99 (t, $^3J_{HH}$ = 8 Hz, 2H, H^6), 7.93 (t, $^3J_{HH}$ = 8 Hz, 2H, H$^{6'}$), 7.51 (d, $^3J_{HH}$ = 6 Hz, 2H, H^8), 7.32−7.26 (m, 4H, H^7, H$^{8'}$), 7.17−7.12 (m, 2H, H$^{7'}$), 2.39 (s, 3H, CH_3). ^{13}C{^{1}H} NMR (CD_3CN): δ = 172.4 (s, NHCOCH$_3$), 160.6 (s, COOC$_6$F$_5$), 157.8 (2s, C^4, C$^{4'}$), 157.0 (s, C^3), 154.8 (s, C$^{3'}$), 152.8 (s, C$^{8'}$), 152.3 (s, C^8), 147.3 (s, C$^{1'}$), 138.7 (s, C^6), 138.4 (s, C$^{6'}$), 131.6 (s, C^1), 128.3 (s, C$^{7'}$), 127.6 (s, C^7), 125.1 (s, C$^{5'}$), 124.8 (s, C^5), 123.4 (s, C^2), 113.5 (s, C$^{2'}$), 24.0 (s, NHCOCH$_3$), (carbon signals of C_6F_5 not observed).[74] ^{19}F NMR (CD_3CN): δ = −73.3 (d, $^1J_{FP}$ = 707 Hz, 12F, PF$_6$), −154.8 (d, $^3J_{FF}$ = 17 Hz, 2F, *o*-F), −159.0 (t, $^3J_{FF}$ = 21 Hz, 1F, *p*-F), −163.8 (dd, $^3J_{FF}$ = 21, 17 Hz, 2F, *m*-F).

Synthesis of ***3***$(PF_6)_4$. [(C_6F_5OOC-tpy)Ru(tpy-NHCOCH$_3$)](PF$_6$)$_2$ **7**(PF$_6$)$_2$ (59.5 mg, 0.053 mmol) and [(EtOOC-tpy)Ru(tpy-NH$_2$)]-(PF$_6$)$_2$ **5**(PF$_6$)$_2$ (50 mg, 0.053 mmol) were each dissolved separately in acetonitrile (10 mL) under an atmosphere of argon and left to stand overnight over activated molecular sieves (3 Å) to remove crystal water. The solution of **5**(PF$_6$)$_2$ then was added to a solution of phosphazene base *tert*-butylimino-tris(dimethylamino)phosphorane (25.8 mg, 0.110 mmol) in absolute acetonitrile (5 mL) and stirred for 45 min followed by the addition of the solution of **7**(PF$_6$)$_2$. After it was stirred at room temperature for 4 h, the reaction was quenched by the addition of a few drops of acetic acid and concentrated under reduced pressure to 5 mL. The product was precipitated by addition of NH_4PF_6 (423 mg) and water (80 mL) and collected via filtration. The crude product was recrystallized from an ethanol/acetone mixture (20 mL, 3:1) and dried under reduced pressure to give [(EtOOC-tpy)Ru(tpy-NHCO-tpy)Ru(tpy-NHCOCH$_3$)](PF$_6$)$_4$ **3**(PF$_6$)$_4$ as red powder. Yield: 78.2 mg (0.042 mmol, 79%). Anal. Calcd for $C_{66}H_{50}F_{24}N_{14}O_4P_4Ru_2$ (1885.2)·4H$_2$O: C, 40.50; H, 2.99; N, 10.02. Found: C, 40.61; H, 2.95; N, 9.78%. MS (ESI$^+$): m/z (%) = 309.0 (5) [M-4PF$_6$-Et-Ac]$^{4+}$, 435.1 (15) [M-4PF$_6$−H]$^{3+}$, 725.1 (29) [M-3PF$_6$−H]$^{2+}$, 777.1 (6) [M-2PF$_6$−Ac]$^{2+}$, 798.1 (100) [M-2PF$_6$]$^{2+}$, 1741.3 (15) [M-PF$_6$]$^+$. HR-MS (ESI$^+$, m/z): calcd. for $C_{66}H_{50}F_{12}N_{14}O_4P_2Ru_2$ [M-2PF$_6$]$^{2+}$: 792.0788; found: 792.0782. ^{1}H NMR (CD_3CN): δ = 10.42 (s, 1H, tpy-CONH-tpy), 9.49 (s, 1H, CONHCH$_3$), 9.36 (s, 2H, H$^{2'}$), 9.34 (s, 2H, H$^{2''}$), 9.23 (s, 2H, H^2), 9.01 (s, 2H, H$^{2'''}$), 8.75 (d, $^3J_{HH}$ = 8 Hz, 2H, H$^{5''}$), 8.70 (d, $^3J_{HH}$ = 8 Hz, 2H, H^5), 8.54 (d, $^3J_{HH}$ = 8 Hz, 2H, H$^{5'}$), 8.44 (d, $^3J_{HH}$ = 8 Hz, 2H, H$^{5'''}$), 8.11−7.89 (m, 8H, H^6, H$^{6'}$, H$^{6''}$, H$^{6'''}$), 7.62−7.50 (m, 4H, H^8, H$^{8''}$), 7.44−7.33 (m, 4H, H$^{8'}$, H$^{8'''}$), 7.33−7.26 (m, 4H, H^7, H$^{7''}$), 7.24−7.14 (m, 4H, H$^{7'}$, H$^{7'''}$) 4.67 (q, 2H, $^3J_{HH}$ = 7 Hz, OCH$_2$CH$_3$), 2.39 (s, 3H, NHCOCH$_3$), 1.59 (t, 3H, $^3J_{HH}$ = 7 Hz, OCH$_2$CH$_3$). ^{13}C{^{1}H} NMR (CD_3CN): δ = 171.6 (s, NHCOCH$_3$), 165.3 (s, tpy-CONH-tpy), 165.1 (s, tpy-COOEt), 158.8, 158.8, 158.7, 158.7, (s, C^4, C$^{4'}$, C$^{4''}$, C$^{4'''}$), 157.5 (s, C$^{3''}$), 157.4 (s, C^3), 156.3 (s, C$^{3'}$), 156.0 (s, C$^{3'''}$), 153.9, 153.8 (s, C$^{8'}$, C$^{8'''}$), 153.5, 153.4 (s, C^8, C$^{8''}$), 148.2 (s, C$^{1'''}$), 147.4 (s, C$^{1'}$), 140.0 (s, C$^{1''}$), 139.5, 139.4 (s, C$^{6'}$, C$^{6'''}$), 139.2, 139.2 (s, C^6, C$^{6''}$), 137.5 (s, C^1), 129.0 (s, C$^{7''}$), 128.9 (s, C^7), 128.7 (s, C$^{7'}$), 128.6 (s, C$^{7'''}$), 125.9 (s, C^5), 125.8 (s, C$^{5''}$), 125.6 (s, C$^{5'}$), 125.5 (s, C$^{5'''}$), 123.8 (s, C^2), 122.7 (s, C$^{2''}$), 115.2 (s, C$^{2'}$), 114.0 (s, C$^{2'''}$), 63.9 (s, OCH$_2$CH$_3$), 24.9 (s, NHCOCH$_3$), 14.7 (s, OCH$_2$CH$_3$).

General Procedure for Removal of Crystal Water from the Complexes ***4***$(PF_6)_2$ *and* ***3***$(PF_6)_4$. The complex (100 mg) was suspended in chlorotrimethylsilane (5 mL) in an atmosphere of dry argon and left to stand for 15−20 min. After removal of excess silane and the formed siloxane under reduced pressure, the complex was dissolved in absolute acetonitrile (5 mL) and dried under reduced pressure again to remove residual acid. NMR analysis showed slight

dx.doi.org/10.1021/ic5020362 | Inorg. Chem. 2014, 53, 12947−12961

downfield shifts of amide proton resonances indicative of traces of remaining hydrochloric acid that could not be removed with this method.

RESULTS AND DISCUSSION

Synthesis of Dinuclear Amide. The dinuclear ruthenium complex $\mathbf{3}^{4+}$ is extremely challenging to synthesize via amide coupling in a classical fashion because of the poor reactivity of the pyridylamine coordinated to the electron-withdrawing ruthenium(II), which is further augmented by the Coulombic repulsion of the doubly charged mononuclear precursors. The pyridylamine can be viewed as an iminium-like structure (= NH_2^+) with rather acidic properties that can be deprotonated using strong bases.[19,31,36] Another possibility to acylate the amino group is by employing acid chlorides at elevated temperatures.[57]

The synthesis of the dinuclear dipeptide $\mathbf{3}^{4+}$ was effected in a four-step synthesis starting from the ethyl ester of the ruthenium amino acid $\mathbf{5}^{2+}$. The first step was acidic cleavage of the ester to the amino acid $\mathbf{1}^{2+}$.[31] Subsequent acetylation of the amino function with acetyl chloride leads to *N*-acetyl amido acid $\mathbf{6}^{2+}$ in a yield of 95%.[57] For the amide coupling of the two building blocks $\mathbf{5}^{2+}$ and $\mathbf{6}^{2+}$ to $\mathbf{3}^{4+}$ suitable conditions needed to be established. A broad range of typical conditions for amide couplings is known,[75] most of which employ active esters in different forms such as 1-hydroxybenzotriazolyl esters (OBt esters),[76−78] 1-hydroxy-7-azabenzotriazolyl esters (OAt esters),[79] pentafluorophenyl esters (OPfp esters),[80,81] and *p*-nitrophenylesters.[82] Intermediate activation can be achieved using acid chlorides[83] or *N*,*N*′-dicyclohexylcarbodiimide (DCC) adducts[84] as active species. More advanced and forcing activation procedures use aminium or phosphonium salt based coupling reagents.[77,78,85] We have recently shown that intermediate activation of ruthenium amino acids and coupling to amino-functionalized ferrocenes, ruthenium complexes, and bipyridines can be achieved using HOBt/DCC,[31] PyBOP,[57] and HATU,[39] respectively, when a strong base, typically a phosphazene base (P_1-*t*Bu) is present (PyBOP = benzotriazol-1-yl-oxytripyrrolidinophosphonium hexafluorophosphate; HATU = 1-[bis(dimethylamino)methylene]-1*H*-1,2,3-triazolo-[4,5-*b*]pyridinium 3-oxide hexafluorophosphate). The latter conditions even distinguish between aromatic amines and the pyridylamine present in the ruthenium amino acid $\mathbf{1}^{2+}$, so that protection of the amino group of the complex is obsolete.[39]

In this work the active ester is isolated and purified to provide a well-defined starting material for the following amide coupling. Pentafluorophenol (PfpOH) is used in combination with *N*,*N*′-diisopropylcarbodiimide to activate the acid. The corresponding urea formed during the reaction is soluble in the water/acetonitrile mixture of the aqueous workup and thus is easily separated from the insoluble OPfp ester $\mathbf{7}^{2+}$. The procedure is generalizable and also applicable to the amino acid $\mathbf{1}^{2+}$ affording the OPfp ester $\mathbf{8}^{2+}$. This active ester does not exhibit any reactivity toward the free pyridylamino group present in the compound itself but rapidly reacts with aliphatic amines such as *tert*-butylamine giving the corresponding amide $\mathbf{9}^{2+}$ (for experimental procedures and ^{1}H and ^{13}C NMR spectra see Supporting Information, Figures S1 and S2).

The dried active ester $\mathbf{7}^{2+}$ readily reacts with the water-free amino ester $\mathbf{5}^{2+}$ after deprotonation of its amino function with P_1-*t*Bu at ambient conditions in reasonable reaction times (4 h). Removal of residual crystal water in the starting materials was accomplished via storage of the respective compounds dissolved in acetonitrile over 3 Å molecular sieves prior to setting up the reaction. During the coupling reaction a striking color change from red to purple was observed, which is attributed to the deprotonation of the generated dinuclear species (vide infra). Neither cleavage of the terminal ester nor the amine function was observed under the given water-free conditions (by NMR and ESI-MS).

The synthesis of the corresponding protected mononuclear complex with identical capping functionalities $\mathbf{4}^{2+}$ was carried out via a literature-known procedure in good yields (Scheme 2).[57]

Characterization of Mono- and Dinuclear Amides. The successful formation of the pentafluorophenylesters of $\mathbf{6}^{2+}$ and $\mathbf{1}^{2+}$ is easily evidenced in the ^{1}H NMR spectra of $\mathbf{7}^{2+}$ and $\mathbf{8}^{2+}$ because the resonances of the protons H^2 are shifted downfield by ∼0.15 ppm. This is attributed to the stronger electron-withdrawing effect of the OPfp group compared to the free carboxylic acid or its ethyl ester (see Schemes 1 and 2 for atom numbering). The remainder of the ^{1}H NMR spectra is rather unaffected from carboxylic acid activation. For example, in $\mathbf{7}^{2+}$ the amide proton resonates at 9.54 ppm, and proton $H^{2'}$ resonates at 9.01 ppm; for $\mathbf{8}^{2+}$, the protons of NH_2 and $H^{2'}$ are found at 6.04 and 8.00 ppm, respectively, which does not differ significantly from the parent compounds $\mathbf{1}^{2+}$ and $\mathbf{6}^{2+}$ (Supporting Information, Figures S3 and S6). ^{13}C NMR chemical shifts (Supporting Information, Figures S4 and S7) are easily assigned via ^{1}H^{13}C correlated techniques (except for the C_6F_5 carbon signals, which are not detected under the given measurement settings). ^{19}F NMR spectroscopy confirms the presence of a perfluorinated phenyl ring as well as of two PF_6 counterions at typical chemical shifts (Supporting Information, Figures S5 and S8). ESI$^+$ mass spectra confirm the integrity of the OPfp esters $\mathbf{7}^{2+}$ and $\mathbf{8}^{2+}$ since only signals of intact cations with no or one counterions are observed.

As expected the NMR spectra of the dinuclear species $\mathbf{3}^{4+}$ are more complicated (Figure 1 and Supporting Information, Figures S9 and S10). The intended high electronic similarity of both complex subunits leads to a multitude of overlapping or close-lying resonances in both the ^{1}H and the ^{13}C NMR spectra. Nevertheless the success of the amide coupling reaction is most easily evidenced by the downfield shift of proton $H^{2'}$ by ∼1.3 ppm now resonating at 9.36 ppm because the influence of the electron-donating amino group is lost. Four sets of signals consisting of one singlet, two doublets, and two doublets of doublets (ignoring ^4J contributions) are expected with intensities of 1:1:1:1 originating from the four different terpyridine moieties present in $\mathbf{3}^{4+}$. Especially the four singlets (protons H^2, $H^{2'}$, $H^{2''}$, and $H^{2'''}$) are sufficiently separated and confirm the successful formation of $\mathbf{3}^{4+}$ (Figure 1). Significant downfield shifts of the proton resonances of the bridging ligand are observed due to the enhanced positive charge of $\mathbf{3}^{4+}$ and the stronger electron-withdrawing effect affecting particularly protons $H^{2'}$ and $H^{2''}$. The high charge also affects the amide proton of the bridging amide: its resonance appears at 10.42 ppm and is shifted by 0.93 ppm compared to the terminal amide proton. In the high-field region of the spectrum the expected singlet of the acetyl group and quartet/triplet pattern of the ethyl ester group are observed at 2.39 and 4.67/1.59 ppm with correct integral ratios, respectively. Despite the overlapping of several signals full assignment of all ^{1}H and ^{13}C resonances was possible using ^{1}H^{13}C correlation spectroscopy.

dx.doi.org/10.1021/ic5020362 | Inorg. Chem. 2014, 53, 12947−12961

Scheme 1. Pentafluorophenylester (OPfp Ester) Formation of Ruthenium Amino Acid $1(PF_6)_2$ and Its Acetyl Amide $6(PF_6)_2$ Leading to $7(PF_6)_2$ and $8(PF_6)_2$ and Subsequent Amidation of $8(PF_6)_2$ with *tert*-Butylamine to $9(PF_6)_2$[a]

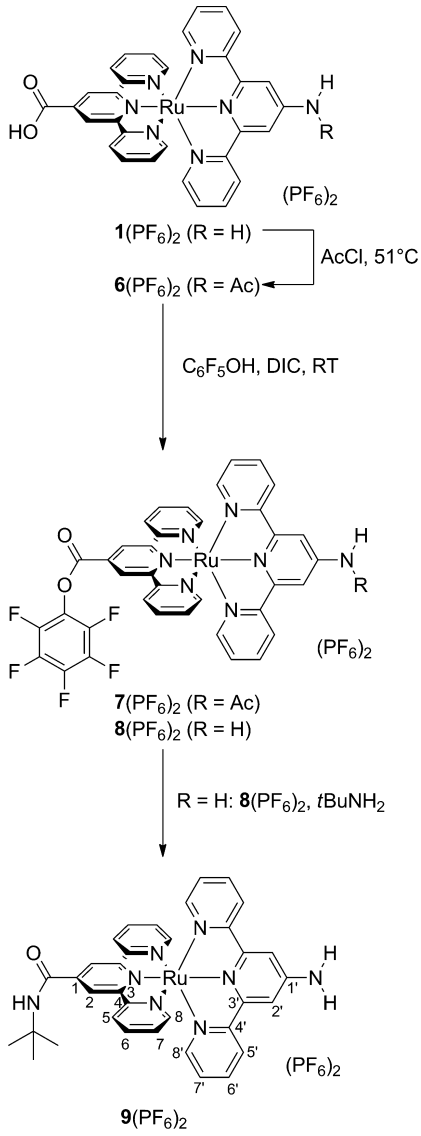

[a]Atom numbering for NMR assignment included.

ESI$^+$ mass spectra further confirm the formation of 3^{4+}. Peaks attributable to $[M\text{-}PF_6]^+$, $[M\text{-}2PF_6]^{2+}$, $[M\text{-}3PF_6\text{–}H]^{2+}$, and $[M\text{-}4PF_6\text{–}H]^{3+}$ dominate the mass spectrum. Presumably the proton that is lost is the bridging amide proton since its acidity is substantially increased due to the neighboring positively charged complex subunits (vide infra). Lower intensity signals of fragments lacking the acetyl and/or ethyl groups are observed as well. Since no other evidence for cleavage of the terminal amide and/or ester could be found, this fragmentation is believed to occur just during desolvation in the aerosol or during the ionization process. IR spectroscopy also reveals the integrity of the dinuclear complex 3^{4+}. The NH and OH stretching vibrations from the amide groups and residual water show up at 3407 and 3649 cm^{-1}. The ester and amide I carbonyl stretching vibrations appear as overlapping bands between 1723 and 1691 cm^{-1}. Additionally the amide groups show typical NH deformation bands (amide II) at 1604 and 1589 cm^{-1}. The PF_6^- counterions are responsible for a broad intense band at 840 cm^{-1}.

Spectroscopic Properties of Mono- and Dinuclear Amides. Both the mono- and the dinuclear bis(terpyridine)-ruthenium(II) complexes 4^{2+} and 3^{4+} exhibit a characteristic ^{1}MLCT transition in the UV–vis/NIR (NIR = near-infrared) absorption spectrum at ~500 nm (Figure 2). For the mononuclear complex 4^{2+} this band is located at 492 nm in good agreement with wavelengths observed for similar bis(terpyridine)ruthenium(II) complexes carrying amido- and carboxylic acid functionalities.[31,37,57] For the dinuclear system 3^{4+} this band is significantly shifted bathochromically to 504 nm. This shift can be attributed to the enhanced push–pull situation caused by the additional charge-carrying complex fragment on the one hand and to the enlarged conjugated aromatic π system on the other, both lowering the energy difference between the highest occupied and the lowest unoccupied orbital (HOMO–LUMO gap). This also affects the extinction coefficient of the ^{1}MLCT band of 3^{4+}. The band is shifted hyperchromically and cannot be described as a simple superposition of two similar but independent bis(terpyridine)-ruthenium-based chromophores. The intraligand π–π^* transitions in the UV region of the absorption spectra of 4^{2+} and 3^{4+}, on the other hand, are very similar in shape and position to those of 3^{4+} being roughly twice as intense as those of 4^{2+}, which is in very good agreement with the doubled number of terpyridine ligands present in 3^{4+}.

DFT calculations employing B3LYP as functional and LANL2DZ as basis set with acetonitrile as solvent in a polarized continuum model (IEFPCM) support the spectroscopic observations and assignments. The visible region is dominated mainly by two transitions, one originating from Ru^{II} → tpy-CO transitions showing up at 490 nm for 3^{4+} and at 476 nm for 4^{2+}, consistent with the trend of the experimental ^{1}MLCT absorption maxima. The other band is based on transitions from Ru^{II} into the more electron-rich tpy-NH ligands and is consequently found at higher energies (435 nm for 3^{4+}, 431 nm for 4^{2+}). This is in good agreement with the observed high-energy shoulders in the ^{1}MLCT bands for both compounds.

Both mononuclear 4^{2+} as well as dinuclear 3^{4+} are emissive at room temperature in fluid solution with emission quantum yields in the range of other bis(terpyridine)ruthenium(II) amino acid derivatives (Table 1, Figure 2). The quantum yield of dinuclear 3^{4+} is lower than that of 4^{2+} by a factor of 2. This might be attributed to the presence of a strongly polarized amide proton in the bridging ligand, which could allow for a more efficient radiationless deactivation pathway. The emission energy of 3^{4+} is shifted slightly bathochromically with respect to 4^{2+} matching the trend in the absorption spectra, which again supports the assumption of a smaller HOMO–LUMO gap in 3^{4+}.

While the asymmetric shape of the emission band of 4^{2+} at room temperature is typical for a ruthenium-based emission, the band shape of 3^{4+} is significantly different: it is more symmetric and has a plateaulike maximum with nearly unchanged emission intensity over a range of 20 nm (Figure 2). On the other hand, the low-temperature emission spectra of 4^{2+} and 3^{4+} in a solid *n*PrCN matrix have essentially the same shape with maxima of 657 and 660 nm, respectively, and a pronounced shoulder at ~720 nm originating from a vibronic progression (Figure 3). We attribute this unusual room-temperature emission behavior to the coexistence of two

dx.doi.org/10.1021/ic5020362 | Inorg. Chem. 2014, 53, 12947–12961

Scheme 2. Amide Coupling of Amino Acid Ester $5(PF_6)_2$ and Acetyl Amido Acid Pentafluorophenyl (OPfp) Ester $7(PF_6)_2$ Giving Dinuclear Complex $3(PF_6)_4$ and Acylation of $5(PF_6)_2$ Leading to the Reference Compound $4(PF_6)_2$[a]

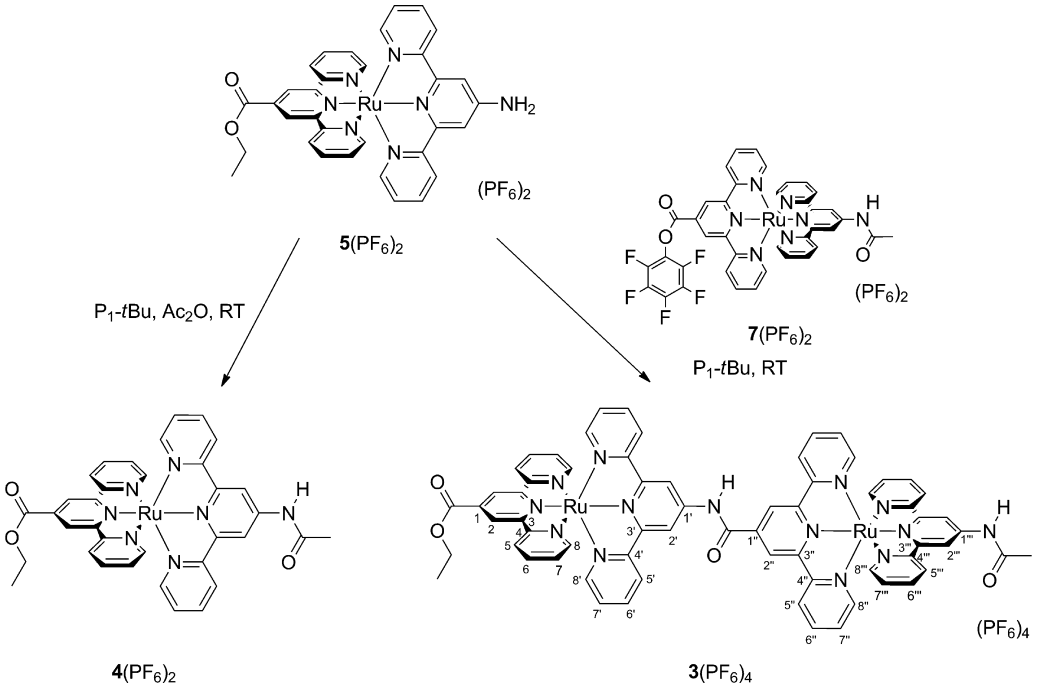

[a]Atom numbering of $3(PF_6)_4$ for NMR assignment included.

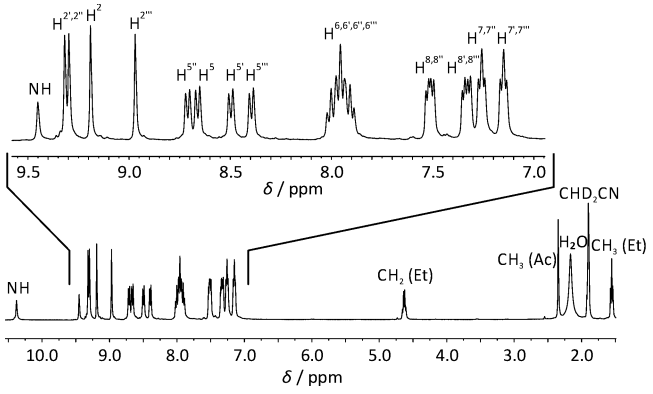

Figure 1. ^1H NMR spectrum of $3(PF_6)_4$ in CD_3CN (lower), aromatic region (upper).

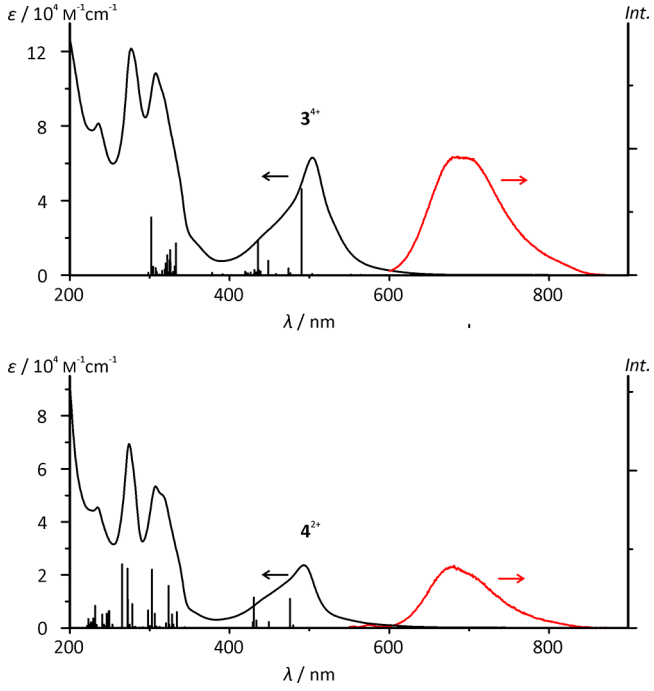

Figure 2. Experimental UV−vis absorption and normalized emission spectra of 3^{4+} (upper) and 4^{2+} (lower) at room temperature in deaerated CH_3CN including oscillator strengths of computed optical transitions (time-dependent DFT: B3LYP, LANL2DZ, IEFPCM: CH_3CN).

emissive triplet states in 3^{4+}. This is in good agreement with the emission lifetimes of both complexes at room temperature. While 4^{2+} exhibits an essentially monoexponential excited-state decay (the second component with 5% relative intensity is likely due to a strongly emissive but otherwise elusive impurity), the excited-state decay of 3^{4+} is clearly biexponential.[86]

The room-temperature emission spectrum of the dinuclear complex 3^{4+} can be fit by a simple superposition of two bands mimicking the emission band shape of a mononuclear complex. This was accomplished using the emission spectrum of 4^{2+} twice at appropriate energies (676 and 705 nm, see Figure 4). The quality of this fit using weighing fractions of 71:29 for the two components, as indicated by the different measured emission lifetimes (Table 1), compared to the emission spectrum of 3^{4+} is remarkable. This allows us to assign the 676 nm emission to τ = 24 ns (71%) and the low energy emission (705 nm) to τ = 44 ns (29%).

Furthermore, we were interested in the dependence of the shape of the emission spectrum of 3^{4+} and hence the ratio of the emitting states as a function of the excitation wavelength (Supporting Information, Figure S11). The emission intensity follows that of the absorption spectrum, and the band shape is

dx.doi.org/10.1021/ic5020362 | Inorg. Chem. 2014, 53, 12947−12961

Table 1. Absorption and Emission Properties in Deaerated CH_3CN at Room Temperature and Emission Properties of 3^{4+} and 4^{2+} in Deaerated *n*PrCN at 77 K

	λ_{max} (^{1}MLCT) (ε)	$\lambda_{Em.}$ ($\lambda_{Exc.}$) at 298 K	$\lambda_{Em.}$ ($\lambda_{Exc.}$) at 77 K	Φ^a	τ^b (contribution)
4^{2+}	492 (22 100)	678 (492)	657 (499)	5.9×10^{-4}	21 (95); 58 (5)
3^{4+}	504 (63 000)	684 (504)	660 (507)	3.2×10^{-4}	24 (71); 44 (29)

[a]Quantum yields Φ are determined at room temperature and given as fraction of emitted photons per absorbed photons. [b]Emission lifetimes τ were determined at the respective emission maxima (λ_{max}/nm; ε/M^{-1} cm^{-1}; $\lambda_{Em.}$/nm; $\lambda_{Exc.}$/nm; τ/ns, contribution/%).

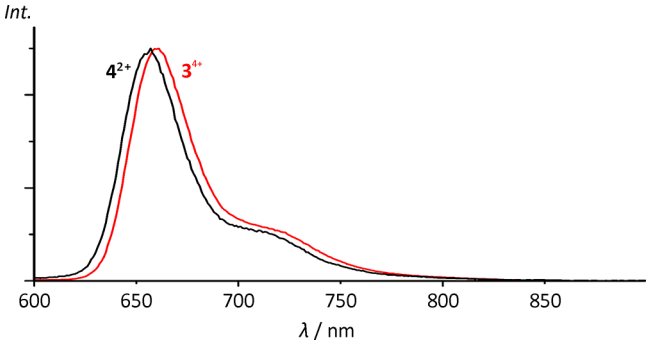

Figure 3. Normalized emission spectra of 3^{4+} (red line) and 4^{2+} (black line) at 77 K in butyronitrile.

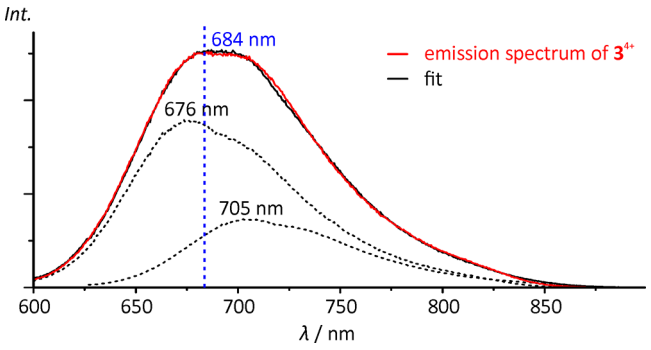

Figure 4. Normalized emission spectrum of 3^{4+} at room temperature in deaerated CH_3CN (red line), emission spectrum of 4^{2+} (dashed lines) shifted to λ_{max} = 676 nm (contribution: 71%) and 705 nm (contribution: 29%), and their sum (solid black line). The blue vertical line indicates the detection wavelength of the emission lifetime measurements.

independent from the irradiation energy. As the relative abundances of the two emissive species are obviously independent from λ_{exc}, the two excited states are in thermal equilibrium in 3^{4+}. As at 77 K only single emission is observed, both emissive states must be connected via a reaction path on the triplet hypersurface with a very low activation barrier to allow for thermal equilibration at room temperature and at 77 K state prior to emission.[87]

To allow for a rapid thermal exchange between the two relevant excited states even at low temperatures the transition between the two emissive states may only involve minor geometric changes. As an exciton transfer between the spatially separated ^{3}MLCT states involving Ru^{III}(tpy$^{\bullet-}$-CONH) and Ru^{III}(tpy$^{\bullet-}$-COOEt) requires the reorganization of various bond lengths the activiation barrier between such two states is expected to be high. Accordingly, this process is unlikely to occur rapidly at 77 K in a frozen matrix, and these two states are ruled out as an origin for the dual emission. If such ^{3}MLCT states with a large activation barrier in between were involved in the emission process dual rather than a single emission would be expected also at low temperatures. Consequently, the two emissive states likely involve Ru^{II} → bridge-tpy-CO triplet states of both Ru^{II} sites due to the spatial proximity of the involved centers.

Although the real electronic situation certainly is more complicated the simplified one-electron orbital representation in Scheme 3 helps to illustrate the processes leading to the observed dual emission. Four different excited states involving the bridging ligand and the two ruthenium centers of 3^{4+} can be thought of according to this diagram. In this simple picture the four conceivable triplet states can be regarded as a $Ru^{III}Ru^{II}$ mixed-valent system with a radical anion as bridging ligand.

Scheme 3. Schematic Illustration of the Four ^{3}MLCT and ^{3}CS Excited States of 3^{4+} Involving the Bridging Ligand[a]

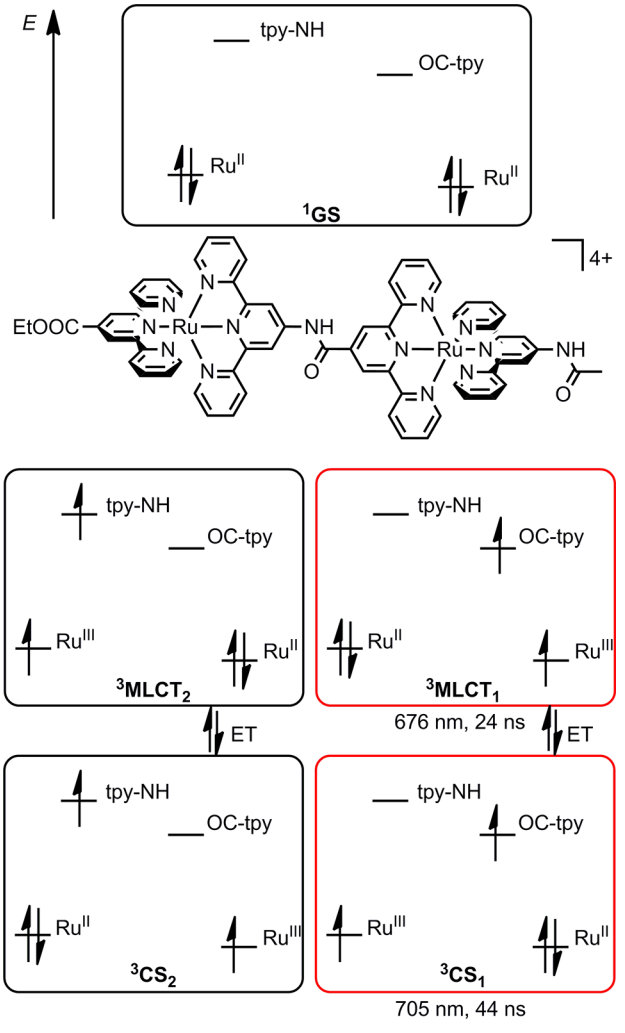

[a]The two electron configurations marked in red are most likely those involved in the room temperature emission of 3^{4+}.

dx.doi.org/10.1021/ic5020362 | Inorg. Chem. 2014, 53, 12947−12961

Two of these triplet states include an odd electron on the tpy-NH fragment of the bridge with one having the character of an MLCT state ($^3MLCT_2$) and the other one having charge-separated state character ($^3CS_2$). Because of the electron-donating effect of the −NH functionality their energies are substantially higher than those of the other two states involving the OC-tpy$^{\bullet-}$ moiety ($^3CS_1$ and $^3MLCT_1$). Consequently only the latter are relevant for excited-state emission according to Kasha's rule.[87] Electron transfer between the two ruthenium centers connects the two excited states $^3CS_1$ and $^3MLCT_1$, which are thus valence-isomeric states. Since $^3CS_1$ features a larger distance between the sites of the excited electron and the Ru^{III} center, recombination/relaxation to the ground state might be slower. This fits to the assignment of a larger lifetime for $^3CS_1$ (τ = 44 ns) as compared to that of $^3MLCT_1$ (τ = 24 ns). The lowest-energy excited triplet state of $\mathbf{3}^{4+}$ was modeled by DFT calculations (B3LYP, LANL2DZ). Its spin density is localized on the bridging OC-tpy and the adjacent Ru^{III} center (Supporting Information, Figure S12), which agrees with studies on the site of the first oxidation (experimental and theoretical, vide infra) and reduction (theoretical, vide infra). Hence triplet $\mathbf{3}^{4+}$ is described as an excited-state mixed-valent system ([Ru^{II}(tpy-NHCO-tpy$^{\bullet-}$)Ru^{III}]/[Ru^{III}(tpy-NHCO-tpy$^{\bullet-}$)Ru^{II}]) of Robin−Day class II exhibiting substantial electronic coupling after optical population of a Ru^{II}-bridge$^{\bullet-}$-Ru^{III} state.

Dual emission of polypyridine ruthenium(II) complexes has been observed very rarely. In mononuclear heteroleptic complexes it usually only arises with electronically very different π-accepting ligands such as in [Ru(bpy)$_2$(phen-4-R)]$^{2+}$ (phen = 1,10-phenanthroline, R = phenylalkynyl)[88] allowing for two ^{3}MLCT states with a high activation barrier in between so that both excited states emit simultaneously at room temperature and at 77 K.[89−91] Alternatively the presence of ^{3}MLCT states as well as intraligand CT states (^{3}ILCT) can be responsible for dual emission in bis(tridentate)ruthenium(II) complexes.[92] In dinuclear ruthenium(II) complexes dual emission has also been observed previously based on two ^{3}MLCT states involving either phen or bpy as accepting ligands.[93] To the best of our knowledge no similar observation of dual emission of dinuclear complexes originating from two Ru^{III}-tpy$^{\bullet-}$ triplet states involving the bridging ligand has been reported before. For a series of dinuclear bis(terpyridine)ruthenium(II) complexes, however, with either back-to-back or *para*-phenylene linkage ([(4′-tolyl-tpy)Ru(tpy-(C_6H_4)$_n$-tpy)Ru(tpy-4′-tolyl)]$^{4+}$ (n = 0, 1, 2) it was shown that partial charge delocalization within the excited triplet state is responsible for a substantial extension of the luminescence lifetime (up to τ = 570 ns, n = 0) along with a bathochromic shift of the emission just as observed in the case of $\mathbf{3}^{4+}$.[94]

Acid−Base Chemistry of the Dinuclear Amide $\mathbf{3}^{4+}$. While the acid−base chemistry of various derivatives of the mononuclear bis(terpyridine)ruthenium(II) amino acid has been previously discussed,[19,31] new reactivity arises from the dinuclear complex $\mathbf{3}^{4+}$ with two amides and a 4+ charge. The strongly polarizing effect of the 2-fold positively charged complex fragments on the bridging amide renders its proton significantly more acidic so that it can be readily abstracted using mild bases such as aliphatic tertiary amines in H_2O/CH_3CN mixtures. The two possible NH deprotonation reactions of $\mathbf{3}^{4+}$ have been studied via NMR and UV−vis absorption spectroscopy employing the strong phosphazene base P_1-*t*Bu under water-free conditions. In the UV−vis absorption spectra (Figure 5) a two-step process is observed with two independent sets of isosbestic points, namely, at 512,

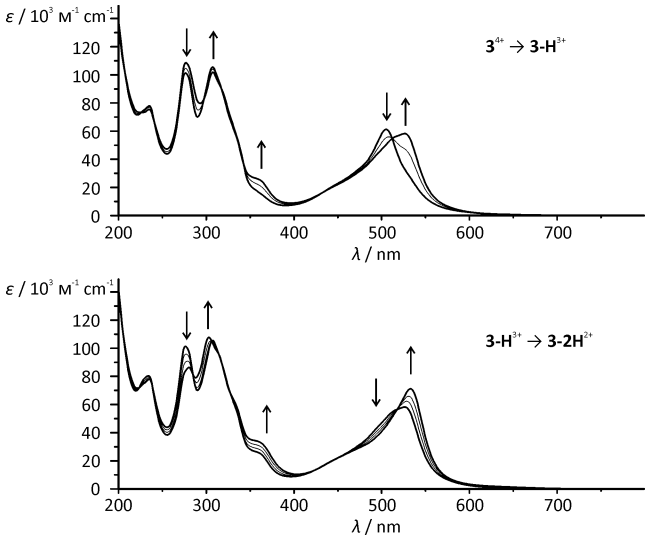

Figure 5. UV−vis absorption spectra of $\mathbf{3}^{4+}$ in dry CH_3CN upon titration with a solution of phosphazene base P_1-*t*Bu in CH_3CN (upper) 0 equiv → 1 equiv leading to $\mathbf{3\text{-}H}^{3+}$, (lower) 1 equiv → 2.5 equiv leading to $\mathbf{3{-}2H}^{2+}$. Arrows indicate most dominant spectral changes.

432, 343, 318, 297, 240, and 225 nm for the first step and at 519, 425, 326, 315, 306, 284, 239, and 223 nm for the second one. This observation is straightforwardly interpreted as the stepwise deprotonation of the complex with the first proton abstraction occurring at the strongly polarized bridging amide giving $\mathbf{3\text{-}H}^{3+}$ and the second one at the terminal $NHCOCH_3$ amide generating $\mathbf{3{-}2H}^{2+}$. Notably, the second deprotonation is not accessible in the presence of water. The bathochromic shift of the ^{1}MLCT absorption band from 504 nm in $\mathbf{3}^{4+}$ to 533 nm in $\mathbf{3{-}2H}^{2+}$ upon deprotonation is reflected by a color change from red to purple (vide supra) and can be traced back to changes in the geometry of the bridging ligand. As suggested by DFT calculations (B3LYP, LANL2DZ, IEFPCM: acetonitrile; vide infra) the tpy-NHCO-tpy bridge planarizes with dihedral angles at the bridging amide of ∼0° after deprotonation. This allows for a stronger π conjugation within the bridge leading to an enlargement of the chromophore and a lowering of the ligand-based LUMO energies. Additionally, the donor strength of the *N*-substituted terpyridine of the bridge is increased raising the energy of the ruthenium-based HOMO.

Support for a stepwise deprotonation mechanism is also obtained from ^{1}H NMR spectroscopy (Figure 6). Upon addition of 1 equiv of P_1-*t*Bu to a solution of $\mathbf{3}^{4+}$ in CD_3CN the resonance of the bridging amide proton at 10.5 ppm disappears, and several other resonances are shifted significantly with respect to the spectrum of $\mathbf{3}^{4+}$. Major changes are observed for the resonances of the bridging ligand tpy-NHCO-tpy with the resonances of the tpy-NH fragment being shifted downfield, while the resonances of the tpy-CO fragment are found further upfield. This can be explained considering the stronger electron-donating effect of tpy-N$^-$ compared to tpy-NH increasing the electron density in this terpyridine. On the other side, the lowered dihedral angle (from −25° to 0°) between the carbonyl group and the proximal terpyridine increases the overlap of the π orbitals of these two fragments

dx.doi.org/10.1021/ic5020362 | Inorg. Chem. 2014, 53, 12947−12961

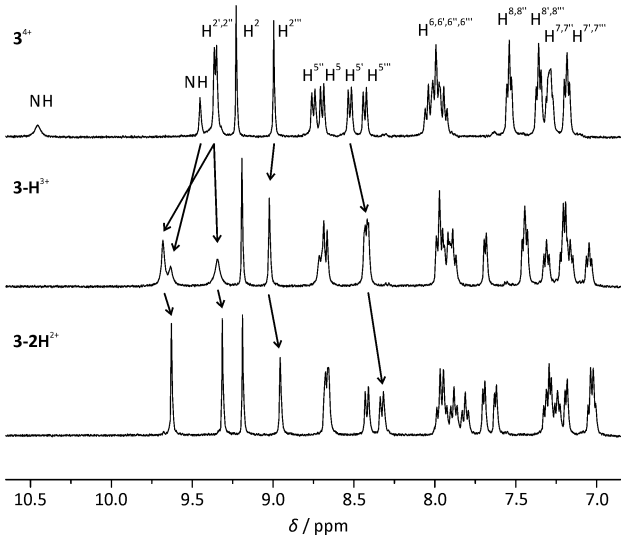

Figure 6. ^{1}H NMR spectra of $\mathbf{3}^{4+}$ in CD_3CN (upper), after addition of 1 equiv of phosphazene base P_1-*t*Bu (center; $\mathbf{3\text{-}H}^{3+}$) and after addition of 2 equiv of phosphazene base P_1-*t*Bu (lower; $\mathbf{3{-}2H}^{2+}$). Arrows indicate shifts upon deprotonation.

resulting in a stronger −M effect of the carbonyl group. Upon addition of a second equivalent of base the resonance of the terminal amide proton disappears, and all aromatic signals are shifted upfield, except for those of the terminal tpy-COOEt ligand, which remain essentially unaltered. This is in agreement with an overall increase of the electron density within the complex upon deprotonation of the terminal amide. The pronounced acidity of the bridging amide will be relevant for the ground- and excited-state redox potentials of $\mathbf{3}^{4+}$ as well.

Redox Properties of Mono- and Dinuclear Amides. The cyclic voltammograms of $\mathbf{3}^{4+}$ and $\mathbf{4}^{2+}$ in CH_3CN have a very similar shape (Figure 7, Table 2). Both complexes show a

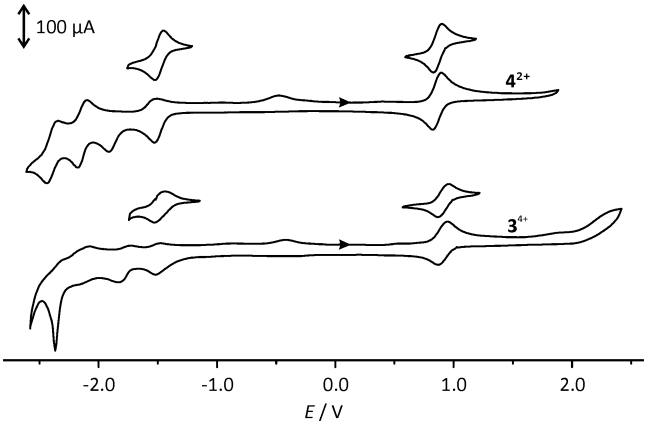

Figure 7. Cyclic voltammograms of 1 mM $\mathbf{4}^{2+}$ (upper) and $\mathbf{3}^{4+}$ (lower) in CH_3CN with 0.1 M $[n\text{Bu}_4][\text{NPF}_6]$ as supporting electrolyte referenced against the FcH/FcH^+ couple. The first oxidation and reduction waves are shown individually.

reversible oxidation wave at ∼0.9 V versus FcH/FcH^+. For $\mathbf{4}^{2+}$ this wave represents the one-electron oxidation of Ru^{II} to Ru^{III} at 0.85 V. In $\mathbf{3}^{4+}$ both Ru^{II} centers are oxidized virtually at the same potential, leading to a two-electron oxidation wave at 0.91 V (referenced against 2 equiv of ferrocene as internal standard in the square-wave voltammogram, Supporting Information, Figure S13). The slightly higher oxidation potential of $\mathbf{3}^{4+}$ compared to that of $\mathbf{4}^{2+}$ may be attributed to the unfavorable charge accumulation in $\mathbf{3}^{4+}$ (double oxidation affords a 6-fold positive charge). Interestingly, no separation of the oxidation waves of the two ruthenium centers is observed indicating no or only weak interaction between the metal sites using $[n\text{Bu}_4\text{N}][\text{PF}_6]$ as electrolyte[95−97] although potential differences are poor measures of electronic coupling.[98−101] Additionally $\mathbf{4}^{2+}$ exhibits four one-electron reduction waves, with the first two being reversible and the second two being quasireversible when examined individually. These are attributed to tpy/tpy$^-$ and tpy$^-$/tpy^{2-} reductions starting with the acceptor-substituted tpy-COOEt ligand. In contrast, $\mathbf{3}^{4+/2+}$ shows only one reversible reduction wave, which accounts for a transfer of two electrons (referenced against internal ferrocene). It occurs essentially at the same potential as the first reduction of the mononuclear system $\mathbf{4}^{2+/+}$ (−1.49 V vs −1.46 V) and therefore is attributed to tpy/tpy$^-$ reductions of both tpy-CO ligands. The second reduction is a quasireversible two-electron reduction ($\mathbf{3}^{2+/0}$). All further reductions overlap significantly so that a clear separation into individual reduction waves is impossible.

The irreversible peak at ca. −0.5 V is a common feature of the cyclic voltammograms (CVs) of both complexes under study. It only arises in the CVs after reducing the respective compounds at potentials below −2.0 V (quasi-reversible). Hence, it arises from the reoxidation of follow-up products of the reduced or doubly reduced state (vide infra for detailed discussion).

As can be seen from the oxidation potentials of $\mathbf{4}^{2+}$ and $\mathbf{3}^{4+}$ (Table 2), a strong oxidant is required to perform the oxidation of $Ru^{II} \rightarrow Ru^{III}$. Only few chemical redox reagents such as Ce^{IV} in acidic aqueous solution ($E_{1/2}$ = 1.3 V in $HClO_4$, 0.88 V in H_2O)[63] and the tris(2,4-dibromophenyl)aminium radical cation[102] in acetonitrile ($E_{1/2}$ = 1.14 V)[63] are capable to do so in a clean fashion. Reproducible UV−vis spectroscopic examination of the oxidation of $\mathbf{4}^{2+}$ and $\mathbf{3}^{4+}$ to $\mathbf{4}^{3+}$ and $\mathbf{3}^{6+}$, respectively, was only possible in 0.5 M H_2SO_4(aq) employing excess $Ce(SO_4)_2$ as oxidant (Figure 8). A set of six isosbestic points is observed for the oxidation of $\mathbf{3}^{4+}$ to $\mathbf{3}^{6+}$ at 556, 421, 338, 298, 285, and 267 nm, indicative of a clean transformation without accumulation of $\mathbf{3}^{5+}$. Even though an excess of oxidant is used, no additional band at ∼400−420 nm is observed originating from remaining Ce^{IV}, which is obviously consumed entirely immediately after addition. The ^{1}MLCT absorption band of $\mathbf{3}^{4+}$ disappears completely, while a new broad and weak band appears with a maximum at 574 nm and a shoulder at ∼720 nm. The disappearance of the ^{1}MLCT band indicates the complete oxidation of both Ru^{II} centers to Ru^{III} under these conditions. The new band is consequently ascribed to a ^{1}LMCT transition from the donor-substituted tpy-NH ligand to Ru^{III}. Its intensity is rather low compared to, for example, the ^{1}LMCT of $[(\text{HOOC-tpy})\text{Ru}^{III}(\text{tpy-NH}_2)]^{3+}$ due to the less-pronounced donor effect of −NHAc as compared to that of $-NH_2$.[19,57] Performing the oxidation of $\mathbf{4}^{2+}$ to $\mathbf{4}^{3+}$ under the same conditions proved to be difficult since on the time scale of recording of the UV−vis absorption spectrum (minutes) after partial oxidation with Ce^{IV} substantial decomposition of the product was observed (absence of isosbestic points, loss of intensity). Only by addition of 10 equiv of oxidant followed by rapid measurement a reproducible spectrum of $\mathbf{4}^{3+}$ could be obtained (Figure 8, lower). It resembles that of the fully oxidized dinuclear complex $\mathbf{3}^{6+}$ (^{1}LMCT band, maxima at 590

dx.doi.org/10.1021/ic5020362 | Inorg. Chem. 2014, 53, 12947−12961

Table 2. Ground- and Excited-State Electrochemical Properties of 4^{2+} and 3^{4+} in 0.1 M $[n\mathrm{Bu}_4][\mathrm{NPF}_6]/\mathrm{CH}_3\mathrm{CN}$ at Room Temperature[a]

	E_{ox} (Ru^{II}/Ru^{III})	$E_{red,1}$ (tpy/tpy$^-$)	$E_{red,2}$ (tpy/tpy$^-$)	E^*_{ox} (Ru^{II}/Ru^{III})[b]	$E^*_{red,1}$ (tpy/tpy$^-$)[c]
4^{2+}	0.85 (68)	−1.46 (73)	−1.86	−1.04	0.43
3^{4+}	0.91 (84, 2e$^-$)	−1.49 (81, 2e$^-$)	−1.78 (2e$^-$)	−0.97	0.39

[a]The peak-to-peak separations ΔE_{pp} of the first oxidation and reduction waves are given in parentheses (E, V vs FcH/FcH^+ ($E_{1/2}$ (FcH/FcH^+) = 0.40 V vs SCE), ΔE_{pp}, mV). [b]$E^*_{ox} = E_{ox} - E_{00}$. [c]$E^*_{red} = E_{red} + E_{00}$. E_{00} determined from emission spectra at 77 K.

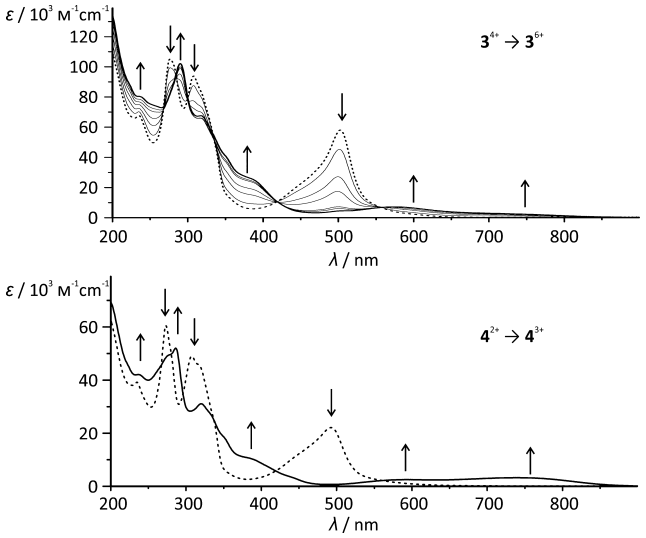

Figure 8. (upper) UV−vis absorption spectra of 3^{4+} in 0.5 M H_2SO_4(aq) upon titration with a solution of $Ce(SO_4)_2$ in 0.5 M H_2SO_4(aq) (0 equiv → approximately 8 equiv). Arrows indicate spectral changes. (lower) UV−vis absorption spectra of 4^{2+} and 4^{3+} for comparison, obtained under the same conditions. Dashed lines indicate spectra of 3^{4+} and 4^{2+}, and bold lines show Ru^{III} complexes 3^{6+} and 4^{3+}.

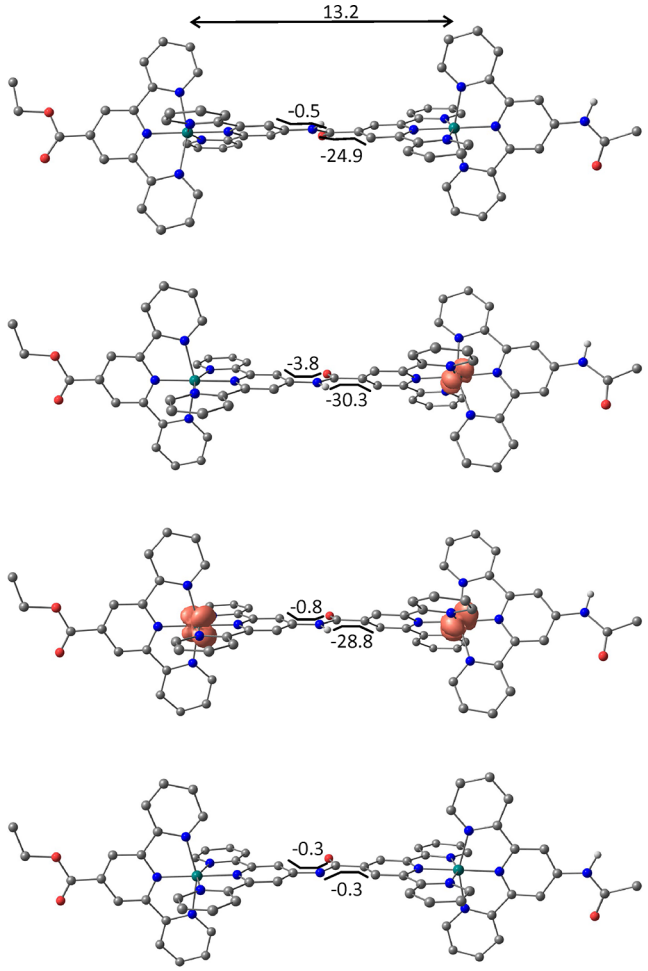

Figure 9. DFT (B3LYP, LANL2DZ, IEFPCM: acetonitrile) optimized geometric structures of 3^{4+}, 3^{5+}, 3^{6+}, and **3-H**$^{3+}$ (upper to lower), including tpy-NHCO-tpy dihedral angles (deg), Ru−Ru distance (Å), and calculated spin densities of 3^{5+} (doublet) and 3^{6+} (triplet). Contour value: 0.01, CH hydrogen atoms are omitted.

and 739 nm) once again underlining the chemical similarity of 4^{2+} and 3^{4+}.

The mixed-valent Ru^{II}−Ru^{III} species 3^{5+} is obtained in a statistical mixture with 3^{4+} and 3^{6+} due to facile disproportionation (2 $Ru^{II}Ru^{III}$ ⇌ $Ru^{II}Ru^{II}$ + $Ru^{III}Ru^{III}$; statistical ratio of 1:2:1 for 3^{4+}:3^{5+}:3^{6+}). During the oxidation of 3^{4+} to 3^{6+}, no band attributable to an intervalence charge-transfer (IVCT) transition is observed in the NIR region of the spectrum up to 1350 nm (solvent absorption beyond 1350 nm prevented recording at longer wavelengths). Oxidation of 3^{4+} in acetonitrile with substoichiometric amounts of tris(2,4-dibromophenyl)aminium hexachloroantimonate did not show the appearance of a new IVCT band in the range between 1000 and 3000 nm. This is in agreement with results from cyclic voltammetry and allows the interpretation of 3^{5+} as a valence-localized mixed-valent cation without observable electronic interaction between the ruthenium centers in different oxidation states (Robin−Day class I).[45,48,52,101,103]

This interpretation is in accordance with DFT calculations (B3LYP, LANL2DZ, IEFPCM: CH_3CN) of the mixed-valent 3^{5+} and the $Ru^{III}Ru^{III}$ 3^{6+} complex (Figure 9). Spin density calculations performed on 3^{5+} localize the unpaired electron on the *N*-terminal ruthenium atom. Upon oxidation to the $Ru^{III}Ru^{III}$ species 3^{6+} spin density is found on both metal centers. Time-dependent calculations on 3^{5+} performed on the same level of theory predict no intensity for IVCT transitions of any kind in the NIR spectral region. Geometry optimizations failed to afford the valence-tautomeric mixed-valent $Ru^{II}Ru^{III}$ cation 3^{5+} with the *C*-terminal ruthenium center being oxidized in repeated attempts suggesting that the $Ru^{II}Ru^{III}$ species is lower in energy.

To further probe the hypothesis of noninteracting ruthenium centers and to localize the electron-hole oxidation, experiments were performed employing paramagnetic ^{1}H NMR spectroscopy. 3^{4+} was titrated with substoichiometric amounts of tris(2,4-dibromophenyl)aminium hexachloroantimonate as oxidant in deuterated acetonitrile (Figure 10). Paramagnetic line broadening and upfield shifts are observed only for certain proton resonances, namely, those assigned to the *N*-terminal bis(terpyridine)ruthenium(II) fragment. Especially pronounced is the shift of the resonances of $H^{2''}$, $H^{2'''}$, and the bridging NH (highlighted with blue boxes in Figure 10), but also the proton resonances of $H^{5''}$, $H^{6''}$, $H^{7''}$, $H^{8''}$, $H^{5'''}$, $H^{6'''}$, $H^{7'''}$, and $H^{8'''}$

dx.doi.org/10.1021/ic5020362 | Inorg. Chem. 2014, 53, 12947−12961

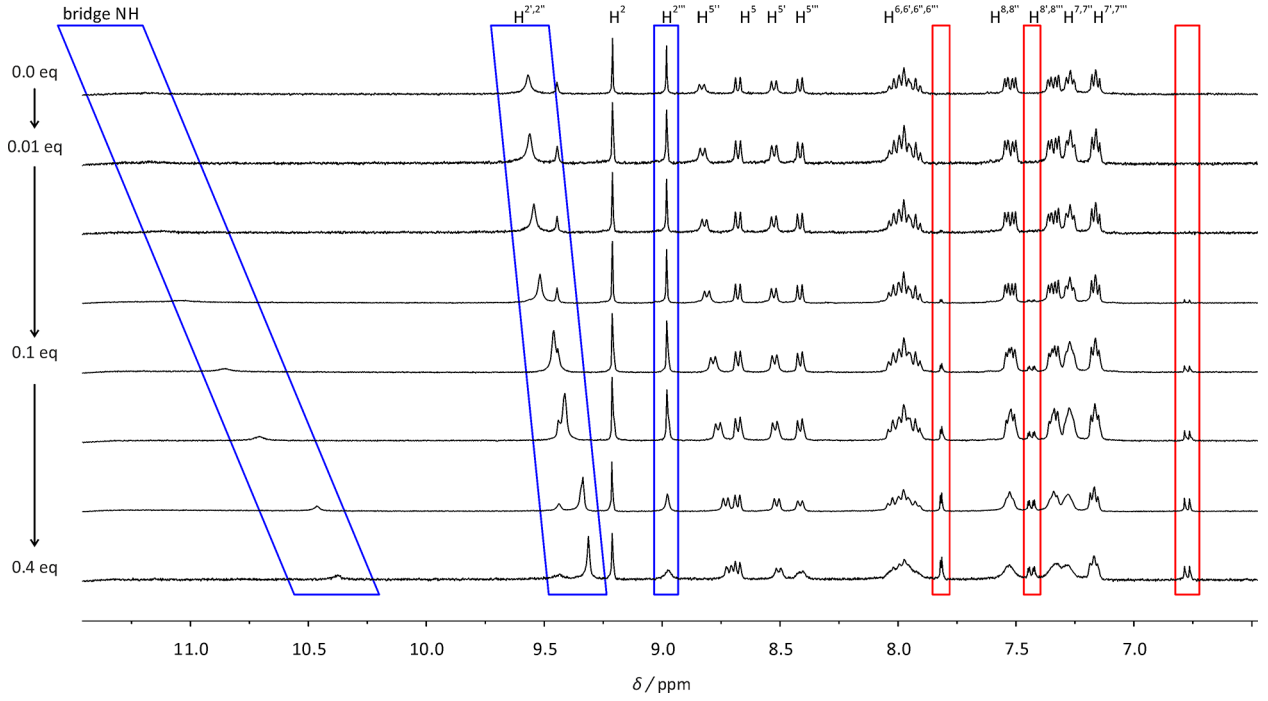

Figure 10. ^{1}H NMR spectra of $\mathbf{3}^{4+}$ in CD_3CN upon partial oxidation to $\mathbf{3}^{5+}$ with substoichiometric amounts of tris(2,4-dibromophenyl)aminium hexachloroantimonate (resonances of the corresponding amine in red frames). Blue frames highlight most significant spectral changes.

respond to the partial oxidation of $\mathbf{3}^{4+}$. At higher concentrations of oxidant (>0.2 equiv) substantial broadening of the proton signals of the *C*-terminal complex fragment also becomes visible because then the concentration of the $Ru^{III}Ru^{III}$ complex $\mathbf{3}^{6+}$ becomes spectroscopically significant due to disproportionation. The observation of the *N*-terminal bis(terpyridine)-ruthenium(II) fragment being the site of the first oxidation agrees with the theoretical results discussed above (Figure 9).

While a clean chemical oxidation of $\mathbf{3}^{4+}$ and $\mathbf{4}^{2+}$ is challenging to accomplish, the ligand-based reductions can easily be carried out using an acetonitrile solution of decamethylcobaltocene ($E_{1/2}$ = −1.91 V).[63] The ligand-centered radicals generated upon addition of 0.9 equiv of $CoCp^*_2$ are examined using EPR spectroscopy after rapid-freezing to 77 K (Figure 11). The EPR spectra of the singly reduced species $\mathbf{3}^{3+}$ and $\mathbf{4}^{+}$ are strikingly similar. Both show a rhombic signal pattern with one *g* value

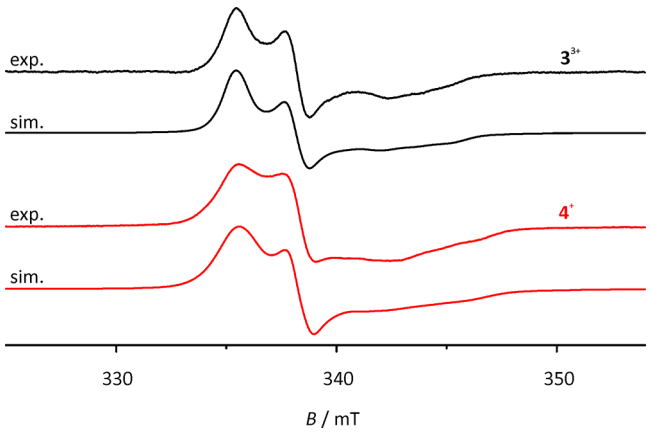

Figure 11. X-band EPR spectra of $\mathbf{3}^{3+}$ (black) and $\mathbf{4}^{+}$ (red) in dry CH_3CN at 77 K after reduction with 0.9 equiv of $CoCp^*_2$ including simulations.

greater and two lower than g_e. This is in agreement with an unpaired electron in the proximity of a low-spin Ru^{II} center. Interestingly, the signal occurring at the highest field is split by a hyperfine coupling to one nitrogen atom giving a 1:1:1 triplet (A (^{14}N) = 15−18 G) suggesting that the unpaired electron is significantly localized on one of the coordinating nitrogen atoms. This is in agreement with the large *g* anisotropy of ~Δ*g* = 0.05 and the substantial superhyperfine coupling to ruthenium required to fit the spectrum (see Table 3), which

Table 3. The *g* Values and Hyperfine and Superhyperfine Coupling Constants *A* of the Unpaired Electron in $\mathbf{4}^{+}$ and $\mathbf{3}^{3+}$ Obtained by Simulation of the Experimental Spectra Recorded in Dry CH_3CN at 77 K Using EasySpin

	$g_{1,2,3}$	Δg^a	$A_{1,2,3}$ (^{99,101}Ru)^b	$A_{1,2,3}$ (^{14}N)^b
$\mathbf{4}^{+}$	2.0045, 1.9885 1.9550	0.0495	2, 10, 24	1, 3, 18
$\mathbf{3}^{3+}$	2.0057, 1.9892, 1.9580	0.0477	2, 8, 15	3, 2.5, 15

$^a\Delta g = g_1 - g_3$. $^b(A, \text{G})$.

is in the range of other nitrogen-based radicals coordinated to a ruthenium(II) ion.[39,40] DFT calculations (B3LYP, LANL2DZ, IEFPCM: acetonitrile) support this interpretation: the spin density of the dinuclear complex $\mathbf{3}^{3+}$ is calculated to be spread mainly on the central pyridyl ring of the bridging tpy-CO ligand with a minor contribution from the coordinated ruthenium center (Supporting Information, Figure S12).

Interestingly, when measuring UV−vis absorption spectra while carrying out the reduction of $\mathbf{4}^{2+}$ and $\mathbf{3}^{4+}$ with up to 4 equiv of $CoCp^*_2$ a clean transition with isosbestic points very similar to those observed upon deprotonation is obtained (Supporting Information, Figure S14). Furthermore, the spectra after addition of an excess of reductant (2 equiv for $\mathbf{4}^{2+}$, 4 equiv for $\mathbf{3}^{4+}$) resemble those of the deprotonated species $\mathbf{4}$-$\mathbf{H}^{+}$ and $\mathbf{3}$-$\mathbf{H}^{3+}$ (see Figure 5). This cannot be interpreted as stepwise reductions of the respective complexes via $\mathbf{4}^{2+} \rightarrow \mathbf{4}^{+} \rightarrow$

dx.doi.org/10.1021/ic5020362 | Inorg. Chem. 2014, 53, 12947−12961

4^0 and $3^{4+} \rightarrow 3^{3+} \rightarrow 3^{2+} \rightarrow 3^{+} \rightarrow 3^0$, respectively, since this should give several sets of isosbestic points in the UV−vis absorption spectra. However, these observations can be easily explained by a follow-up reaction after the initial reduction to 4^+ and 3^{3+} (rapid-freeze EPR), namely, the irreversible reduction of protons to H_2. Alternatively, a direct reduction of protons by decamethylcobaltocene yielding dihydrogen is plausible.[104] The proton source could be residual crystal water generating OH^-, which deprotonates the amides. Excess of reductant is required due to varying amounts of water present in 4^{2+} and 3^{4+} (see Experimental Section). Spectral changes of similar shape have been observed previously with dinuclear amide conjugates in our group upon addition of decamethylcobaltocene as reductant.[39,40] The results obtained in the current study suggest that also in those cases the bridging amide is deprotonated in the presence of H_2O (UV−vis) after initial reduction of the complexes (rapid-freeze EPR).

The same process, namely, deprotonation of 3^{4+}, is observed when monitoring the addition of $CoCp^*_2$ via NMR spectroscopy (slow time scale). No paramagnetic signal broadening appears upon addition of reductant to a solution of 3^{4+} (Supporting Information, Figure S15). This would have been indicative of the presence of a radical anion especially because the expected line broadening of the proton resonances is larger for a ligand-based radical as compared to a metal-based radical (Figure 10). The discrepancy between EPR results, on the one hand, where the unpaired electron originating from a complex-based reduction can be observed, and NMR and UV−vis absorption spectroscopy, on the other hand, which reveal follow-up products of this initial reduction, is ascribed to the different time scales of the respective experiments: because of the apparent instability of the radical formed in the presence of residual H_2O, rapid freezing of the solution of 3^{4+} a few seconds after addition of $CoCp^*_2$ allows detection of an EPR signal, while the NMR and UV−vis absorption measurements are carried out several minutes after the addition of reductant, allowing follow-up reactions to occur prior to measurement. CV experiments further support this interpretation: scanning just the potential range of the first ligand-based reduction of 3^{4+} delivers a reversible redox wave. Scanning the full solvent window requires enough time to allow for further reactions of the complex after reduction. The reoxidation of the follow-up species then occurs at ca. −0.5 V for both complexes 4^{2+} and 3^{4+} shifted by approximately 1 V to more positive values (Figure 7). This lends further support to a reaction sequence $3^{4+} \rightarrow 3^{3+} \rightarrow \mathbf{3\text{-}H}^{3+} + 1/2H_2$.

The excited-state redox potentials of the complexes 4^{2+} and 3^{4+} were calculated from $E_{ox}^* = E_{ox} - E_{00}$ and $E_{red}^* = E_{red} + E_{00}$ (Table 2).[105,106] As expected the complexes become stronger reductants and oxidants in the ^{3}MLCT excited state. To probe the excited-state properties of 4^{2+} and 3^{4+} Stern−Volmer plots with various ferrocene derivatives and amines as potential weak electron donors were recorded (Table 4).[107] Employing ferrocene, ferrocenecarboxylic acid methyl ester, and 1,1′-ferrocenedicarboxylic acid dimethyl ester as electron donors for the reductive quenching of the ^{3}MLCT state of 4^{2+}, linear Stern−Volmer plots are obtained that show a clear dependence of the quenching rate k_q from the redox potential of the corresponding quencher (Supporting Information, Figure S16).[108−111] Lowering the driving force for the electron-transfer step reduces the efficiency of the reductive quenching significantly as expected from Marcus theory. Interestingly even if the electron-transfer step is estimated to be thermodynamically slightly uphill by 70 mV as in the reaction of 4^{2+} with $Fc(COOMe)_2$ very efficient quenching of the emission of 4^{2+} is still observed. This cannot be accounted for solely with a contribution from a reductive electron-transfer step from the ferrocene to the ruthenium complex. An additional feasible path for radiationless deactivation is an energy transfer from the ^{3}MLCT state of the Ru complex populating the nonemissive triplet excited state of the respective ferrocene derivative.[31,112−114] While stronger electron-withdrawing substituents on ferrocene lower its reduction potential, they also stabilize its triplet state facilitating energy transfer. It is worth noting that for both the mono- and the dinuclear complexes 4^{2+} and 3^{4+} very rapid quenching with formal bimolecular rate constants close to the diffusion limit ($k = 1.9 \times 10^{10}$, 298 K, CH_3CN)[115] is observed with all ferrocene derivatives without any detectable static quenching due to preorganization phenomena of the two components in their respective ground states. This emphasizes that a significant contribution of the excited-state quenching by ferrocene originates from energy transfer.

Table 4. Excited-State Stern−Volmer Quenching Constants K_{SV}[a] of 4^{2+} and 3^{4+} by Various Quenchers, Fraction f[b] of Complex Accessible for Quencher, Bimolecular Quenching Rate Constants k_q,[c] and Quenching Fractions η_q[d] by 0.1 M Quencher in CH_3CN at Room Temperature

		4^{2+}	3^{4+}
FcH ($E_{1/2}$ = 0.00 V)[63]	$K_{sv}(f)$	246 (100)	432 (100)
	k_q	1.17×10^{10}	1.80×10^{10}
	η_q	0.96	0.98
FcCOOMe ($E_{1/2}$ = 0.30 V)[125]	$K_{sv}(f)$	160 (100)	
	k_q	7.62×10^9	
	η_q	0.94	
$Fc(COOMe)_2$ ($E_{1/2}$ = 0.50 V)[126]	$K_{sv}(f)$	147 (100)	399 (100)
	k_q	7.00×10^9	1.66×10^{10}
	η_q	0.94	0.98
Ph-NMe_2 ($E_{1/2}$ = 0.39 V)[117]	$K_{sv}(f)$	1.8 (100)	14.4 (57)
	k_q	8.6×10^7	6.00×10^8
	η_q	15	34

[a] K_{SV}, M^{-1}. [b] f, %. [c] k_q, M^{-1} s^{-1} = K_{SV}/τ. [d] η_q, % = $fK_{sv}[Q](1 + K_{sv}[Q])^{-1}$.

The choice of amines as electron sources for reductive electron transfer quenching of the complexes 4^{2+} and 3^{4+} is limited due to the facile deprotonation of the amide protons (vide supra). Using *N*,*N*-dimethylaniline, which is not sufficiently basic to abstract protons from the bridge of 3^{4+} (pK_s = 5.1;[116] substantiated by UV−vis absorption spectroscopy) as electron source ($E_{1/2}$ = 0.39 V vs FcH/FcH^+),[117] it is possible to record Stern−Volmer plots for both complexes 4^{2+} and 3^{4+} (Figure 12). While its quenching efficiency with respect to 4^{2+} is weak (2 orders of magnitude lower than that for $Fc(COOMe)_2$; Table 4) it is increased by almost 1 order of magnitude in the 3^{4+}/amine pair. This cannot be explained just by the marginally increased driving force for the electron transfer by 40 mV (Table 2). Additionally a curve bent downward toward the *x*-axis is obtained when $(I_0/I - 1)$ is plotted against $c_{quencher}$ indicating a precoordination of the quencher to the emissive species (Figure 12). An appropriate plot employing $I_0/(I_0 - I) = (fK_{sv}[Q])^{-1} + f^{-1}$ gives the fraction f of the emissive species actively taking part in the bimolecular quenching process as well as the Stern−Volmer constant K_{sv} (Supporting Information, Figure S17).[118] We ascribe the substantial quenching fraction to an association of

dx.doi.org/10.1021/ic5020362 | Inorg. Chem. 2014, 53, 12947−12961

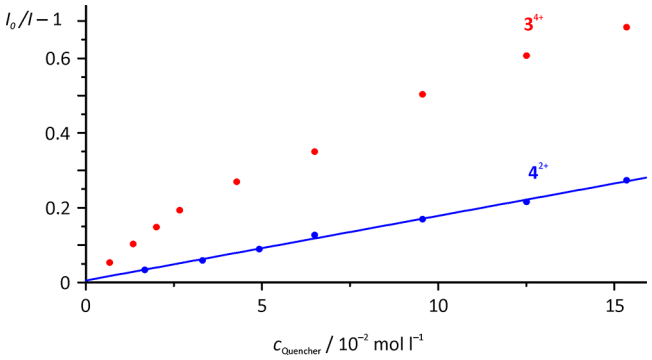

Figure 12. Stern–Volmer plots of the mono- and dinuclear complexes 4^{2+} (blue) and 3^{4+} (red) employing *N*,*N*-dimethylaniline as quencher. Plots were obtained using complex concentrations of $c = 2 \times 10^{-5}$ mol L^{-1}.

the $PhNMe_2$ nitrogen atom to the polarized proton of the bridging amide via a strong hydrogen bond. This facilitates inner-sphere reductive electron transfer into one of the two excited states of the dinuclear complex as illustrated in Scheme 4. Similar observations of precoordination, especially via hydrogen bonds facilitating electron transfer from/to excited states, have been documented in the literature.[119−124]

Scheme 4. Reductive Electron Transfer from $PhNMe_2$ to the Two Excited Triplet States of 3^{4+}

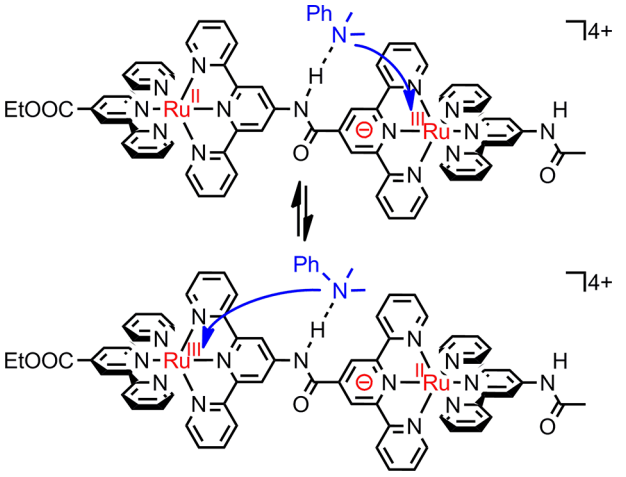

CONCLUSION

The new dinuclear bis(terpyridine)ruthenium(II) complex 3^{4+} with remarkable electronic symmetry despite an asymmetric bridge was synthesized and fully characterized. No electronic coupling is observed in the mixed-valent state 3^{5+}. However, the similarity of the chemical environments of the ruthenium centers in 3^{4+} enables a thermal electron transfer between Ru^{II} and Ru^{III} in the triplet excited states of 3^{4+}. The two valence tautomers are observed via emission spectroscopy (dual emission) and excited-state lifetime measurements.

Reduction of 3^{4+} with $CoCp^*_2$ initially yields the radical localized on the bridge. This radical further reacts to finally give the deprotonated complex **3-H**$^{3+}$ and presumably H_2. **3-H**$^{3+}$ and **3−2H**$^{2+}$ are prepared directly from strong bases and 3^{4+}. $PhNMe_2$ is not basic enough to deprotonate 3^{4+} but coordinates to the bridging NH group via a hydrogen bond, which facilitates reductive electron transfer from $PhNMe_2$ to the excited complex 3^{4+}. Further studies will be conducted to elucidate this process, namely, whether 3^{4+} can act as an electro- or photocatalyst for the reduction of protons from water and which role the proton of the bridging amide plays in such a process.

ASSOCIATED CONTENT

Supporting Information

Experimental procedures for the syntheses of $8(PF_6)_2$ and $9(PF_6)_2$; ^1H and ^{13}C NMR spectra of $7(PF_6)_2$, $8(PF_6)_2$, and $9(PF_6)_2$; ^{19}F NMR spectra of $7(PF_6)_2$ and $8(PF_6)_2$; CH-HSQC and CH-HMBC spectra of $3(PF_6)_4$; emission spectra of $3(PF_6)_4$ at different excitation wavelengths; figures of DFT-optimized geometries of 3^{3+} and triplet 3^{4+}; UV–vis absorption spectra of 3^{4+} and 4^{2+} upon titration with $CoCp^*_2$; ^1H NMR spectra of 3^{4+} upon deprotonation; Stern–Volmer plots of 3^{4+} and 4^{2+} with different ferrocene derivatives; Cartesian coordinates of DFT-optimized geometries of 3^{4+}, 3^{5+}, 3^{6+}, triplet 3^{4+}, and 3^{3+}. This material is available free of charge via the Internet at http://pubs.acs.org.

AUTHOR INFORMATION

Corresponding Author

*Fax: +49613127277. E-mail: katja.heinze@uni-mainz.de.

Author Contributions

The manuscript was written through contributions of all authors. All authors have given approval to the final version of the manuscript.

Funding

This work was financially supported by the Deutsche Forschungsgemeinschaft (GSC 266, Materials Science in Mainz, scholarship for C.K.).

Notes

The authors declare no competing financial interest.

REFERENCES

(1) Sauvage, J. P.; Collin, J. P.; Chambron, J. C.; Guillerez, S.; Coudret, C.; Balzani, V.; Barigelletti, F.; Cola, L.; de Flamigni, L. *Chem. Rev.* **1994**, *94*, 993−1019.
(2) D'Alessandro, D. M.; Keene, F. R. *New J. Chem.* **2006**, *30*, 228−237.
(3) Chiorboli, C.; Indelli, M. T.; Scandola, F. *Top. Curr. Chem.* **2005**, *257*, 63−102.
(4) Sun, L.; Hammarström, L.; Åkermark, B.; Styring, S. *Chem. Soc. Rev.* **2001**, *30*, 36−49.
(5) Barigelletti, F.; Flamigni, L. *Chem. Soc. Rev.* **2000**, *29*, 1−12.
(6) Flores-Torres, S.; Hutchison, G. R.; Soltzberg, L. J.; Abruña, H. D. *J. Am. Chem. Soc.* **2006**, *128*, 1513−1522.
(7) Akasaka, T.; Inoue, H.; Kuwabara, M.; Mutai, T.; Otsuki, J.; Araki, K. *Dalton Trans.* **2003**, 815−821.
(8) Siebler, D.; Linseis, M.; Gasi, T.; Carrella, L. M.; Winter, R. F.; Förster, C.; Heinze, K. *Chem.—Eur. J.* **2011**, *17*, 4540−4551.
(9) Ozawa, H.; Haga, M.; Sakai, K. *J. Am. Chem. Soc.* **2006**, *128*, 4926−4927.
(10) Elvington, M.; Brown, J.; Arachchige, S. M.; Brewer, K. J. *J. Am. Chem. Soc.* **2007**, *129*, 10644−10645.
(11) Takeda, H.; Koike, K.; Inoue, H.; Ishitani, O. *J. Am. Chem. Soc.* **2008**, *130*, 2023−2031.
(12) Kumar, A.; Chhatwal, M.; Mondal, P. C.; Singh, V.; Singh, A. K.; Cristaldi, D. A.; Gupta, R. D.; Gulino, A. *Chem. Commun.* **2014**, *50*, 3783.
(13) O'Regan, B.; Grätzel, M. *Nature* **1991**, *353*, 737−740.

(14) Bolink, H. J.; Cappelli, L.; Coronado, E.; Gaviña, P. *Inorg. Chem.* **2005**, *44*, 5966−5968.
(15) Kalyanasundaram, K. *Coord. Chem. Rev.* **1982**, *46*, 159−244.
(16) Caspar, J. V.; Meyer, T. J. *J. Am. Chem. Soc.* **1983**, *105*, 5583−5590.
(17) Meyer, T. J. *Pure Appl. Chem.* **1986**, *58*, 1193−1206.
(18) Suzuki, K.; Kobayashi, A.; Kaneko, S.; Takehira, K.; Yoshihara, T.; Ishida, H.; Shiina, Y.; Oishi, S.; Tobita, S. *Phys. Chem. Chem. Phys.* **2009**, *11*, 9850−9860.
(19) Breivogel, A.; Kreitner, C.; Heinze, K. *Eur. J. Inorg. Chem.* **2014**, *2014*, 10.1002/ejic.201402466.
(20) Breivogel, A.; Wooh, S.; Dietrich, J.; Kim, T. Y.; Kang, Y. S.; Char, K.; Heinze, K. *Eur. J. Inorg. Chem.* **2014**, 2720−2734.
(21) Biner, M.; Buergi, H. B.; Ludi, A.; Roehr, C. *J. Am. Chem. Soc.* **1992**, *114*, 5197−5203.
(22) Lashgari, K.; Kritikos, M.; Norrestam, R.; Norrby, T. *Acta Crystallogr., Sect. C: Cryst. Struct. Commun.* **1999**, *55*, 64−67.
(23) Calvert, J. M.; Caspar, J. V.; Binstead, R. A.; Westmoreland, T. D.; Meyer, T. J. *J. Am. Chem. Soc.* **1982**, *104*, 6620−6627.
(24) Maestri, M.; Armaroli, N.; Balzani, V.; Constable, E. C.; Thompson, A. M. W. C. *Inorg. Chem.* **1995**, *34*, 2759−2767.
(25) Medlycott, E. A.; Hanan, G. S. *Chem. Soc. Rev.* **2005**, *34*, 133.
(26) Abrahamsson, M.; Jäger, M.; Österman, T.; Eriksson, L.; Persson, P.; Becker, H.-C.; Johansson, O.; Hammarström, L. *J. Am. Chem. Soc.* **2006**, *128*, 12616−12617.
(27) Schramm, F.; Meded, V.; Fliegl, H.; Fink, K.; Fuhr, O.; Qu, Z.; Klopper, W.; Finn, S.; Keyes, T. E.; Ruben, M. *Inorg. Chem.* **2009**, *48*, 5677−5684.
(28) Breivogel, A.; Förster, C.; Heinze, K. *Inorg. Chem.* **2010**, *49*, 7052−7056.
(29) Breivogel, A.; Meister, M.; Förster, C.; Laquai, F.; Heinze, K. *Chem.—Eur. J.* **2013**, *19*, 13745−13760.
(30) Brown, D. G.; Sanguantrakun, N.; Schulze, B.; Schubert, U. S.; Berlinguette, C. P. *J. Am. Chem. Soc.* **2012**, *134*, 12354−12357.
(31) Heinze, K.; Hempel, K.; Beckmann, M. *Eur. J. Inorg. Chem.* **2006**, 2040−2050.
(32) Reynal, A.; Palomares, E. *Eur. J. Inorg. Chem.* **2011**, 4509−4526.
(33) Sun, P.; Krishnan, A.; Yadav, A.; Singh, S.; MacDonnell, F. M.; Armstrong, D. W. *Inorg. Chem.* **2007**, *46*, 10312−10320.
(34) Gong, L.; Mulcahy, S. P.; Harms, K.; Meggers, E. *J. Am. Chem. Soc.* **2009**, *131*, 9602−9603.
(35) Meggers, E. *Chem.—Eur. J.* **2010**, *16*, 752−758.
(36) Heinze, K.; Hempel, K.; Tschierlei, S.; Schmitt, M.; Popp, J.; Rau, S. *Eur. J. Inorg. Chem.* **2009**, 3119−3126.
(37) Heinze, K.; Hempel, K.; Breivogel, A. *Z. Anorg. Allg. Chem.* **2009**, *635*, 2541−2549.
(38) Heinze, K.; Hempel, K. *Chem.—Eur. J.* **2009**, *15*, 1346−1358.
(39) Dietrich, J.; Thorenz, U.; Förster, C.; Heinze, K. *Inorg. Chem.* **2013**, *52*, 1248−1264.
(40) Dietrich, J.; Wünsche von Leupoldt, A.; Grabolle, M.; Resch-Genger, U.; Heinze, K. *Eur. J. Inorg. Chem.* **2013**, 3009−3019.
(41) Hurley, D. J.; Roppe, J. R.; Tor, Y. *Chem. Commun.* **1999**, 993−994.
(42) Bishop, B. M.; McCafferty, D. G.; Erickson, B. W. *Tetrahedron* **2000**, *56*, 4629−4638.
(43) Kise, K. J.; Bowler, B. E. *Inorg. Chem.* **2002**, *41*, 379−386.
(44) Creutz, C.; Taube, H. *J. Am. Chem. Soc.* **1969**, *91*, 3988−3989.
(45) Kaim, W.; Klein, A.; Glöckle, M. *Acc. Chem. Res.* **2000**, *33*, 755−763.
(46) Kaim, W.; Sarkar, B. *Coord. Chem. Rev.* **2007**, *251*, 584−594.
(47) Kaim, W.; Lahiri, G. K. *Angew. Chem.* **2007**, *119*, 1808−1828; *Angew. Chem., Int. Ed.* **2007**, *46*, 1778−1796.
(48) Hush, N. *Electrochim. Acta* **1968**, *13*, 1005−1023.
(49) Fuerholz, U.; Buergi, H. B.; Wagner, F. E.; Stebler, A.; Ammeter, J. H.; Krausz, E.; Clark, R. J. H.; Stead, M. J.; Ludi, A. *J. Am. Chem. Soc.* **1984**, *106*, 121−123.
(50) Zhang, L. T.; Ko, J.; Ondrechen, M. J. *J. Am. Chem. Soc.* **1987**, *109*, 1666−1671.
(51) Hush, N. *Coord. Chem. Rev.* **1985**, *64*, 135−157.
(52) Robin, M. B.; Day, P. *Adv. Inorg. Chem.* **1968**, *10*, 247−422.
(53) Brunschwig, B. S.; Creutz, C.; Sutin, N. *Chem. Soc. Rev.* **2002**, *31*, 168−184.
(54) D'Alessandro, D. M.; Topley, A. C.; Davies, M. S.; Keene, F. R. *Chem.—Eur. J.* **2006**, *12*, 4873−4884.
(55) Crutchley, R. J. *Angew. Chem.* **2005**, *117*, 6610−6612; *Angew. Chem., Int. Ed.* **2005**, *44*, 6452−6454.
(56) Moser, C. C.; Keske, J. M.; Warncke, K.; Farid, R. S.; Dutton, P. L. *Nature* **1992**, *355*, 796−802.
(57) Breivogel, A.; Hempel, K.; Heinze, K. *Inorg. Chim. Acta* **2011**, *374*, 152−162.
(58) Sortino, S.; Petralia, S.; Di Bella, S. *J. Am. Chem. Soc.* **2003**, *125*, 5610−5611.
(59) Weinberg, D. R.; Gagliardi, C. J.; Hull, J. F.; Murphy, C. F.; Kent, C. A.; Westlake, B. C.; Paul, A.; Ess, D. H.; McCafferty, D. G.; Meyer, T. J. *Chem. Rev.* **2012**, *112*, 4016−4093.
(60) Neidlinger, A.; Ksenofontov, V.; Heinze, K. *Organometallics* **2013**, *32*, 5955−5965.
(61) Bordwell, F. G.; Ji, G. Z. *J. Am. Chem. Soc.* **1991**, *113*, 8398−8401.
(62) Fulmer, G. R.; Miller, A. J. M.; Sherden, N. H.; Gottlieb, H. E.; Nudelman, A.; Stoltz, B. M.; Bercaw, J. E.; Goldberg, K. I. *Organometallics* **2010**, *29*, 2176−2179.
(63) Connelly, N. G.; Geiger, W. E. *Chem. Rev.* **1996**, *96*, 877−910.
(64) Stoll, S.; Schweiger, A. *J. Magn. Reson.* **2006**, *178*, 42−55.
(65) Frisch, M. J.; Trucks, G. W.; Schlegel, H. B.; Scuseria, G. E.; Robb, M. A.; Cheeseman, J. R.; Scalmani, G.; Barone, V.; Mennucci, B.; Petersson, G. A.; Nakatsuji, H.; Caricato, M.; Li, X.; Hratchian, H. P.; Izmaylov, A. F.; Bloino, J.; Zheng, G.; Sonnenberg, J. L.; Hada, M.; Ehara, M.; Toyota, K.; Fukuda, R.; Hasegawa, J.; Ishida, M.; Nakajima, T.; Honda, Y.; Kitao, O.; Nakai, H.; Vreven, T.; Montgomery, J. J. A.; Peralta, J. E.; Ogliaro, F.; Bearpark, M.; Heyd, J. J.; Brothers, E.; Kudin, K. N.; Staroverov, V. N.; Kobayashi, R.; Normand, J.; Raghavachari, K.; Rendell, A.; Burant, J. C.; Iyengar, S. S.; Tomasi, J.; Cossi, M.; Rega, N.; Millam, J. M.; Klene, M.; Knox, J. E.; Cross, J. B.; Bakken, V.; Adamo, C.; Jaramillo, J.; Gomperts, R.; Stratmann, R. E.; Yazyev, O.; Austin, A. J.; Cammi, R.; Pomelli, C.; Ochterski, J. W.; Martin, R. L.; Morokuma, K.; Zakrzewski, V. G.; Voth, G. A.; Salvador, P.; Dannenberg, J. J.; Dapprich, S.; Daniels, A. D.; Farkas, Ö.; Foresman, J. B.; Ortiz, J. V.; Cioslowski, J.; Fox, D. J. *Gaussian09*, Rev. A.02; Gaussian, Inc.: Wallingford, CT, 2009.
(66) Becke, A. D. *J. Chem. Phys.* **1993**, *98*, 5648.
(67) Dunning, T. H.; Hay, P. J. in *Methods of Electronic Structure Theory;* Schaefer, H. F., Ed.; Springer: Boston, MA, 1977.
(68) Hay, P. J.; Wadt, W. R. *J. Chem. Phys.* **1985**, *82*, 270.
(69) Wadt, W. R.; Hay, P. J. *J. Chem. Phys.* **1985**, *82*, 284.
(70) Hay, P. J.; Wadt, W. R. *J. Chem. Phys.* **1985**, *82*, 299.
(71) Miertuš, S.; Scrocco, E.; Tomasi, J. *Chem. Phys.* **1981**, *55*, 117−129.
(72) Miertuš, S.; Tomasi, J. *Chem. Phys.* **1982**, *65*, 239−245.
(73) Pascual-ahuir, J. L.; Silla, E.; Tunon, I. *J. Comput. Chem.* **1994**, *15*, 1127−1138.
(74) Rosales, A.; Muñoz-Bascón, J.; López-Sánchez, C.; Álvarez-Corral, M.; Muñoz-Dorado, M.; Rodríguez-García, I.; Oltra, J. E. *J. Org. Chem.* **2012**, *77*, 4171−4176.
(75) Han, S.-Y.; Kim, Y.-A. *Tetrahedron* **2004**, *60*, 2447−2467.
(76) König, W.; Geiger, R. *Chem. Ber.* **1970**, *103*, 788−798.
(77) Coste, J.; Le-Nguyen, D.; Castro, B. *Tetrahedron Lett.* **1990**, *31*, 205−208.
(78) Frérot, E.; Coste, J.; Pantaloni, A.; Dufour, M.-N.; Jouin, P. *Tetrahedron* **1991**, *47*, 259−270.
(79) Carpino, L. A. *J. Am. Chem. Soc.* **1993**, *115*, 4397−4398.
(80) Kisfaludy, L.; Schön, I. *Synthesis* **1983**, *1983*, 325−327.
(81) Atherton, E.; Cameron, L. R.; Sheppard, R. C. *Tetrahedron* **1988**, *44*, 843−857.
(82) Gagnon, P.; Huang, X.; Therrien, E.; Keillor, J. W. *Tetrahedron Lett.* **2002**, *43*, 7717−7719.
(83) Beyermann, M.; Bienert, M.; Niedrich, H.; Carpino, L. A.; Sadat-Aalaee, D. *J. Org. Chem.* **1990**, *55*, 721−728.

(84) Neises, B.; Steglich, W. *Angew. Chem.* **1978**, *90*, 556−557; *Angew. Chem., Int. Ed.* **1978**, *17*, 522−524.
(85) Albericio, F.; Bofill, J. M.; El-Faham, A.; Kates, S. A. *J. Org. Chem.* **1998**, *63*, 9678−9683.
(86) First interpretations of this observation were based on the presence of two different solvates of 3^{4+}, one potentially an H_2O and the other one a CH_3CN solvate (via hydrogen bonds to the NH groups). Another interpretation included the simultaneous presence of contact ion pairs and solvent-separated ion pairs. These contact ion pairs were proposed as the complex cation 3^{4+} and a strongly hydrogen-bonded PF_6^- counterion in the "binding pocket" of the bridging amide functionality as observed for other dinuclear amide-bridged complexes in our group.[39,40] To verify these interpretations lifetime measurements with varying concentrations of H_2O as good solvent and Cl^- ions as competing counterion were performed. These lifetime experiments showed that the ratio of the two emissive species and their emission lifetimes are essentially independent from these parameters excluding an interpretation of this kind.
(87) Kasha, M. *Discuss. Faraday Soc.* **1950**, *9*, 14−19.
(88) Glazer, E. C.; Magde, D.; Tor, Y. *J. Am. Chem. Soc.* **2007**, *129*, 8544−8551.
(89) Chen, Y.; Zhou, X.; Wei, X.-H.; Yu, B.-L.; Chao, H.; Ji, L.-N. *Inorg. Chem. Commun.* **2010**, *13*, 1018−1020.
(90) Siebert, R.; Schlütter, F.; Winter, A.; Presselt, M.; Görls, H.; Schubert, U. S.; Dietzek, B.; Popp, J. *Cent. Eur. J. Chem.* **2011**, *9*, 990−999.
(91) Sen, R.; Koner, S.; Bhattacharjee, A.; Kusz, J.; Miyashita, Y.; Okamoto, K.-I. *Dalton Trans.* **2011**, *40*, 6952.
(92) Song, L.-q.; Feng, J.; Wang, X.-s.; Yu, J.-h.; Hou, Y.-j.; Xie, P.-h.; Zhang, B.-w.; Xiang, J.-f.; Ai, X.-c.; Zhang, J.-p. *Inorg. Chem.* **2003**, *42*, 3393−3395.
(93) Glazer, E. C.; Magde, D.; Tor, Y. *J. Am. Chem. Soc.* **2005**, *127*, 4190−4192.
(94) Hammarström, L.; Barigelletti, F.; Flamigni, L.; Indelli, M. T.; Armaroli, N.; Calogero, G.; Guardigli, M.; Sour, A.; Collin, J.-P.; Sauvage, J.-P. *J. Phys. Chem. A* **1997**, *101*, 9061−9069.
(95) Creutz, C. *Prog. Inorg. Chem.* **1983**, *30*, 1−73.
(96) Richardson, D. E.; Taube, H. *Coord. Chem. Rev.* **1984**, *60*, 107−129.
(97) Crutchley, R. J. *Adv. Inorg. Chem.* **1994**, *41*, 273−325.
(98) LeSuer, R. J.; Buttolph, C.; Geiger, W. E. *Anal. Chem.* **2004**, *76*, 6395−6401.
(99) LeSuer, R. J.; Geiger, W. E. *Angew. Chem.* **2000**, *112*, 254−256; *Angew. Chem., Int. Ed.* **2000**, *39*, 248−250.
(100) D'Alessandro, D. M.; Keene, F. R. *Dalton Trans.* **2004**, 3950.
(101) Winter, R. F. *Organometallics* **2014**, *33*, 4517−4536.
(102) Yueh, W.; Bauld, N. L. *J. Am. Chem. Soc.* **1995**, *117*, 5671−5676.
(103) Hush, N. S. *Prog. Inorg. Chem.* **1967**, *8*, 391−444.
(104) Koelle, U.; Infelta, P. P.; Graetzel, M. *Inorg. Chem.* **1988**, *27*, 879−883.
(105) Rehm, D.; Weller, A. *Ber. Bunsen-Ges.* **1969**, *73*, 834−839.
(106) Bock, C. R.; Connor, J. A.; Gutierrez, A. R.; Meyer, T. J.; Whitten, D. G.; Sullivan, B. P.; Nagle, J. K. *J. Am. Chem. Soc.* **1979**, *101*, 4815−4824.
(107) Stern, O.; Volmer, M. *Phys. Z.* **1919**, *20*, 183−188.
(108) Marcus, R. A. *J. Chem. Phys.* **1956**, *24*, 979−989.
(109) Marcus, R. A. *J. Chem. Phys.* **1956**, *24*, 966−978.
(110) Marcus, R. A. *J. Chem. Phys.* **1965**, *43*, 2654−2657.
(111) Marcus, R. A. *J. Chem. Phys.* **1965**, *43*, 679−701.
(112) Farlow, B.; Nile, T. A.; Walsh, J. L.; McPhail, A. T. *Polyhedron* **1993**, *12*, 2891−2894.
(113) Hutchison, K.; Morris, J. C.; Nile, T. A.; Walsh, J. L.; Thompson, D. W.; Petersen, J. D.; Schoonover, J. R. *Inorg. Chem.* **1999**, *38*, 2516−2523.
(114) Siemeling, U.; Vor der Brüggen, J.; Vorfeld, U.; Neumann, B.; Stammler, A.; Stammler, H.-G.; Brockhinke, A.; Plessow, R.; Zanello, P.; Laschi, F.; Fabrizi de Biani, F.; Fontani, M.; Steenken, S.; Stapper, M.; Gurzadyan, G. *Chem.—Eur. J.* **2003**, *9*, 2819−2833.
(115) McCleskey, T. M.; Winkler, J. R.; Gray, H. B. *J. Am. Chem. Soc.* **1992**, *114*, 6935−6937.
(116) Burk, P.; Ruasse, M.-F.; Kaljurand, I.; Lilleorg, R.; Murumaa, A.; Mishima, M.; Koppel, I.; Koppel, I. A.; Leito, I. *J. Phys. Org. Chem.* **2013**, *26*, 171−181.
(117) Andrew, T. L.; Swager, T. M. *J. Org. Chem.* **2011**, *76*, 2976−2993.
(118) *Principles of Fluorescence Spectroscopy;* Lakowicz, J. R., Ed.; Springer: Boston, MA, 1983.
(119) Tyson, D. S.; Luman, C. R.; Zhou, X.; Castellano, F. N. *Inorg. Chem.* **2001**, *40*, 4063−4071.
(120) Zhao, G.-J.; Liu, J.-Y.; Zhou, L.-C.; Han, K.-L. *J. Phys. Chem. B* **2007**, *111*, 8940−8945.
(121) Huynh, M. H. V.; Meyer, T. J. *Chem. Rev.* **2007**, *107*, 5004−5064.
(122) Wenger, O. S. *Chem.—Eur. J.* **2011**, *17*, 11692−11702.
(123) Nishino, T.; Hayashi, N.; Bui, P. T. *J. Am. Chem. Soc.* **2013**, *135*, 4592−4595.
(124) Wenger, O. S. *Acc. Chem. Res.* **2013**, *46*, 1517−1526.
(125) Abasq, M.-L.; Saidi, M.; Burgot, J.-L.; Darchen, A. *J. Organomet. Chem.* **2009**, *694*, 36−42.
(126) Blankespoor, R. L. *Inorg. Chem.* **1985**, *24*, 1126−1128.